journal of the American Ceramic Society

Machine Learning Interatomic Potentials for Pyrolysis of Polysiloxanes and Properties of SiCO Ceramics

Journal:	*Journal of the American Ceramic Society*
Manuscript ID	JACERS-52833.R1
Wiley - Manuscript type:	Research Article (Direct Via EEO)
Date Submitted by the Author:	n/a
Complete List of Authors:	Falgoust, Mitchell; The University of Texas at Arlington, Chemistry Kroll, Peter; The University of Texas at Arlington, Chemistry
Keywords:	pyrolysis, polymer precursor, molecular dynamics, silicon oxycarbide
Author-supplied Keyword: If there is one additional keyword you would like to include that was not on the list, please add it below::	machine-learning interatomic potentials

SCHOLARONE™
Manuscripts

Machine Learning Interatomic Potentials for Pyrolysis of Polysiloxanes and Properties of SiCO Ceramics

Mitchell Falgoust and Peter Kroll*

Department of Chemistry and Biochemistry, The University of Texas at Arlington,
700 Planetarium Place, Arlington, Texas 76019, United States.

* Corresponding authors: pkroll@uta.edu

For Peer Review

Abstract

We present Machine–Learning Interatomic Potentials (MLIPs) for simulations of Si-C-O-H compounds. The MLIPs are constructed from Moment-Tensor-Potentials (MTPs) and were trained to a library of configurations that included polysiloxane structures, hypothetical crystalline and amorphous SiCOH structures, and trajectories of Si-C-O-H systems obtained via ab-initio molecular dynamic (aiMD) simulations at elevated temperatures. Passive, active, and hybrid learning strategies were implemented to develop the MLIPs.

The MLIPs reproduce vibrational properties of polymers and SiCOH structures obtained from aiMD simulations, thus providing a tool to identify chemical units and distinct structural characteristics through their vibrational properties. Simulations of the polymer-to-ceramic transformation show the development of mixed tetrahedra in SiCO ceramics and align with experimental observations. Million-atom simulations for several nanoseconds highlight the precipitation of graphitic nanosheets from a carbon-rich SiCO precursor. Atomistic simulations with the MLIPs deliver details of chemical reaction mechanisms during the pyrolysis of polysiloxanes, including methane abstraction and Kumada-like rearrangements that transform the siloxane backbone. While the MLIPs still leave room for systematic improvement, they deliver simulations with “DFT-like” quality at low and high temperatures.

1 Introduction

Polymer-derived silicon oxycarbide (SiCO) ceramics are known for high thermal and chemical stability, biocompatibility, intriguing electrical properties at extreme conditions,[1-3] and potential use as anode material for Li^+ or Na^+ storage.[4-5] Porous SiCO can be selectively synthesized with micro-, meso-, and macroporosity and is a membrane material for separations or a vehicle for drug delivery systems.[6-8] The polymer-to-ceramics route is a versatile and robust approach,[9] and many polysiloxanes are applied as SiCOH precursors for polymer-derived ceramics (PDCs). New trends in processing and applications include additive manufacturing and tooth and bone implants.[10-12]

The thermal conversion of a pre-ceramic siloxane polymer into a SiCO ceramic generates various intermediate states, and the temperature and environment atmosphere chosen during processing impact the composition and morphology of the resulting material. Pyrolysis typically occurs between 400 and 1000°C and yields an amorphous SiCO ceramic[2] that comprises a glassy network in which additional "excess" or "free" carbon is embedded. The SiCO glass comprises corner-sharing SiC_nO_{4-n}–tetrahedra (n=1–4), so-called "mixed tetrahedra".[13-14] The "free" carbon phase of SiCO is the source of many of the material's functional properties. Determining the carbonaceous structure in amorphous SiCO and its interface to the surrounding glassy SiCO host is challenging, and various hypotheses have been formulated.[14-16] Further annealing of amorphous SiCO at 1200°C and higher temperatures induces a phase separation of glassy SiCO into SiC and SiO_2.[17] Above ~1350˚C, carbothermal reduction transforms "free" carbon and SiO_2 to SiC, releasing CO.[18] Several excellent reviews address the synthesis, characterization, and properties of SiCO ceramics.[2, 14-15, 19-20]

Over the last two decades, modeling and simulation of SiCO materials addressed structure, enthalpy of formation, and some physical and mechanical properties. [21 16, 22-25] Computational studies of chemical reactions during pyrolysis are a recent topic.[26-28] Constant challenges in these simulations are model size, simulation length, and accuracy of the method

For Peer Review

used. Focusing on SiCO simulations, accurate quantum chemical simulations are limited to a few hundred atoms simulated for not much more than a nanosecond. Empirical interatomic potentials such as the Tersoff potential trade in accuracy for speed, enabling simulations of millions of atoms and extending simulations over microseconds. The reactive force-field (ReaxFF)[28-30] approach is located between these antipodes and promises to deliver accurate descriptions of chemical reactions with the speed of an empirical potential. Each method has its range of applicability, and with time moving on, the range and maximum size will be pushed forward.

Recently, so-called machine–learning interatomic potentials (MLIPs) have proven to be an effective new tool that bridges the gap between accurate quantum chemical and empirical potential simulations. Various approaches to construct MLIPs have been presented in the literature under acronyms such as GAP, SOAP, NNP, GNN, ACE, SNAP, and SchNet – by no means an exhaustive list.[31-38] Characteristic of these MLIPs is a representation of chemical interactions by mathematical descriptors of arbitrary complexity.[39] The ML approaches are usually referred to as "non-parametric" in the sense that when building an MLIP, the focus is on optimizing an objective function rather than involving traditional parameters of bonding and interaction. In this work, we develop MLIPs based on Moment Tensor Potentials (MTPs) introduced by Shapeev.[40] MTPs comprise two-body interactions represented by rotationally and translationally invariant polynomials within a predefined cutoff distance. Three- and multi-body interactions are stored in moments. Increasing the number of basis functions, the number of outer products, or the cutoff distance are paths to improve systematically the accuracy of the MLIP.[40] The parameters of the model are fitted to energies, forces, and stresses – that we computed using density-functional theory (DFT) – for a variety of configurations.

Working with the MTP approach to MLIPs, our first goal of this contribution is to provide a high-fidelity tool to model low-temperature properties of SiCO materials, including elastic and plastic deformations or vibrational signatures of phase segregations. This endeavor succeeds, as the process involves only the configurational sampling of localized bonding environments. Our second goal is more far-reaching: we aim to simulate chemical reactions as

For Peer Review

they occur during the pyrolysis of polysiloxanes. Anticipating our results, we obtain new MLIPs suitable to study distinct reaction mechanisms, including the details of carbon migration into the siloxane backbone. The MLIP is fast enough to perform large–scale (1,000,000 atoms) conversions for several nanoseconds with local accuracy resembling DFT simulations.

2 Computational Method

With our goal to develop machine-learning interatomic potentials (MLIPs) for simulations of structure, low-temperature properties, and high-temperature reactivity of polymers comprising the elements Si, C, O, and H, we use the moment tensor potentials (MTPs) developed by Shapeev.[40] This particular approach has been used successfully to describe structural properties of α-SiO_2, diffusion coefficients for Si, and nano-hardness in large SiC models.[41-44] Consequently, MTPs should also be suitable for simulations of SiCO materials and SiCOH pre-ceramic polymers. A detailed description of the formalisms of the MTP representation can be found elsewhere.[40, 45-46]

To obtain the parameters of MTPs, we perform machine learning (linear regression) using an extensive library of DFT configurations with associated energies, forces, and stresses. The training data is provided to the MLIP-2 software[45] that performs the machine learning. The objective function addresses the difference between target (DFT) and computed (MTP) energies, forces, and stresses. To compose the training data, we tap into our library of distinct SiCOH structures of different compositions that we have accumulated over the last two decades. It includes configurations of various polysiloxanes with standard side groups (H, CH_3, C_5H_6), hypothetical crystalline structures of SiCO with different compositions,[23] models of amorphous SiCO with and without "excess" carbon,[16, 21-22] and trajectories from *ab-initio* molecular dynamic (aiMD) simulations of Si-C-O-H polymers and SiCOH structures at elevated temperatures. Overall, the library covers a configurational space ranging from local minima to snapshots taken from dynamic simulations at 3000 K. We use the built-in active selection functionality of MLIP-2 to select critical configurations and avoid feeding the algorithm with repetition. Hence, we

For Peer Review

systematically improved the training set, focusing on low-temperature configurations first and then augmenting it with configurations at high temperatures. For example, we recently observed fundamental reaction mechanisms (including Kumada-like rearrangements) in aiMD simulations of siloxanes.[47] Significant parts of those trajectories are included in our training set for the MLIPs.

All configurations have been recalculated with identical parameters to obtain consistent energies, forces, and stresses for the machine-learning procedure. We used the Vienna ab initio Simulation Package (VASP)[48-50], with the projector augmented wave (PAW) method[51-52] and the Generalized Gradient Approximation as parametrized by Perdew, Becke, and Ernzerhof (PBE)[53-54] augmented by the universal correction method for dispersion corrections.[55] A cut-off of 500 eV is used to expand the wave function into plane wave basis sets. If structure optimizations are performed, forces are converged to 5 meV/Å for models smaller than 80 atoms and 0.1 eV/Å if larger. The reciprocal space is sampled to better than $0.04 \cdot 2\pi$/Å. We use the Γ-point only for models larger than 80 atoms.

We use passive and active learning strategies integrated within the MLIP-2 software. The passive strategy uses the provided DFT data only and obtains parameters suitable to describe the configurations as provided. For additional "on-the-fly" active learning, the MLIP-2 code interfaces with the LAMMPS [Large-scale Atomic/Molecular Massively Parallel Simulator][56] code to perform molecular dynamic (MD) simulations (NVT, time-step Δt=1 fs). ~~LAMMPS uses a current MLIP estimate and samples new configurations that are potentially fed back to VASP for DFT calculations.~~ The choice of temperature in LAMMPS was T=300 K for low-temperature and T=2500 K for high-temperature simulations.

~~As described above, our training set was built using optimized SiCOH structure models, snapshots from trajectories of dynamical simulations obtained by aiMD at elevated temperatures, and by MD simulations using LAMMPS produced during active learning.~~ We ~~have also~~ implemented another independent ~~MLIP~~LAMMPS-VASP loop as a "self-learning" strategy. [28] ~~The loop passes final configurations generated by MD simulations in LAMMPS (using a current~~

For Peer Review

MLIP) back to VASP for additional aiMD simulations. Subsequently, the final step of that aiMD simulation is passed back to LAMMPS, restarting the sequence. At low temperatures, without bond breaking, such athe loop must provide equivalent local configurations at the end of each methodafter simulations using the MLIP or by aiMD. , whileIdentifying "divergence" of these trajectories and adding selectedidentifies configurations to be added to the training set helped to improve the MLIPs. The settings for the aiMD simulations in this cycle are those mentioned above. A typical length of MD simulations was 100 ps, while the length of aiMD simulations was 1-10 ps depending on model size. After careful selection and further optimization of the procedure concerning efficiency and necessity, the final training set used in this study consists of 3,417 different structures comprising 503,885 atoms (and their forces). Note that this is, on average, 148 atoms per structure.

Gauging the quality of the MLIPs is performed in the following way. The MTP formalism allows various flavors of complexity, resulting in different numbers of parameters in the final MLIP.[45] For instance, the cutoff radius, our final choice is 4.25 Å, impacts the complexity and speed of the MLIP. The main focus here addresses the "level variant" of the MTPs. Ultimately, we settled with a level–12 MTP, but we also developed and worked with level–20, –22, and –26. Levels of the MTPs are related to the number of polynomials used in the MTP, which relate to a proportionate number of parameters. Ultimately, the computational efforts for using MLIPs in MD simulations are proportional to the number of scalar parameters, which are 46, 295, 421, and 706 for level -12, -20, -22, and -26, respectively. Note that these are not the ultimate numbers of parameters to be fitted but a gauge to estimate the effort required. The level-12 MTP we showcase below contains more than 1100 parameters, the level-22 MTP comprises more than ten times as many. For the different level variants, we looked at commonly shared values, such as root mean square (RMS) and maximal absolute difference (MAD) of the error in energy and forces. We compared the results for a specific testing set composed of models obtained during the active learning and "self-learning" cycles. As expected, improvement (indicated by lower RMS and lower MAD) is observed for the most demanding MTP (level 26).

For Peer Review

A practical gauge of comparison is visualized below in Figure 1. It compares the fidelity of force calculations – in the way of differences of force magnitude acting on an atom computed for the same configuration using the two different methods, f_{MTP}–f_{DFT} – for MTPs with level–12, –20, and –22 at low (800 K) and high (2500 K) temperatures. Our choice of the x–y axes facilitates an easy visual alignment of the 2D data to the 1D distribution (histogram) frequently shown.[57]

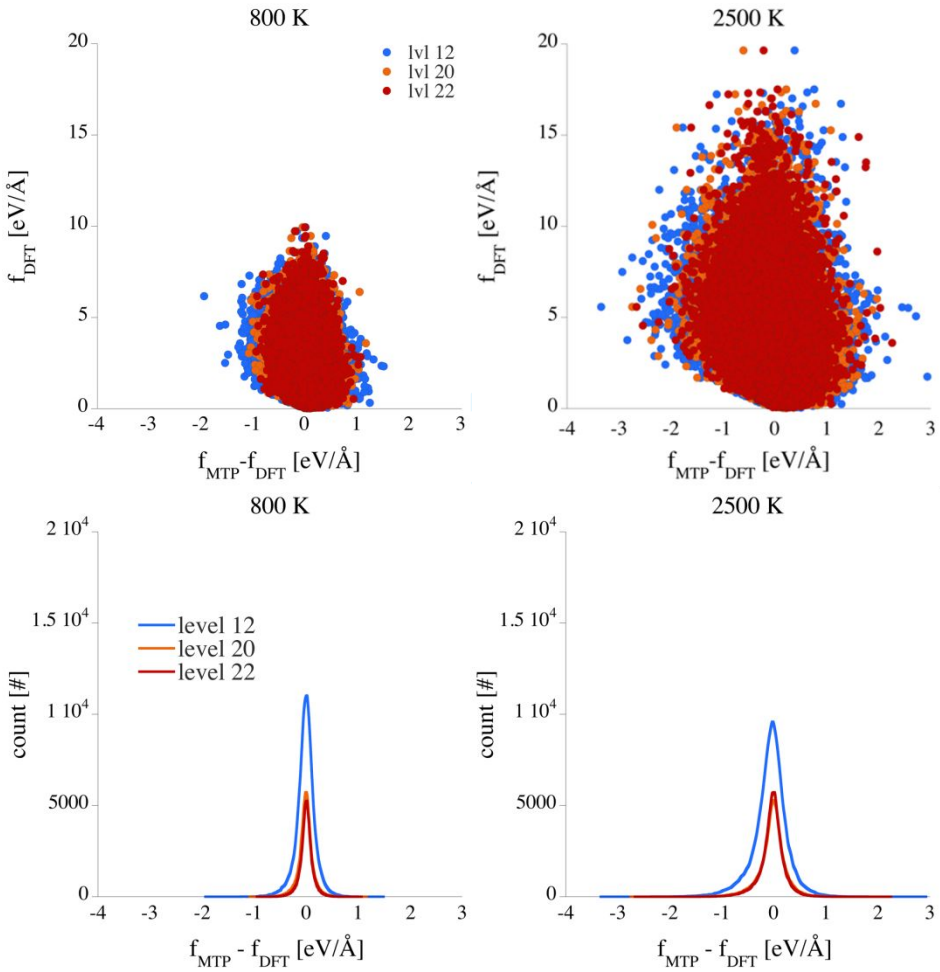

Figure 1: Visualizing DFT force magnitude f_{DFT} versus differences between MTP force magnitude and DFT force magnitude, f_{MTP}–f_{DFT}. The top row shows the data for temperatures of 800 K (left) and 2500 K (right) using individual dots for each data point. The bottom row displays the distribution of the force magnitude difference. The data is generated from the forces acting on each atom collecting several structures. Level–12, –20, and –22 are indicated in blue, orange, and red, respectively. Level–20 and –22 generate virtually identical distributions.

As expected, the fidelity of force calculations (e.g., decrease of the width) increases as the level of the MTP increases. This is seen by a smaller distribution width (bottom row) as the level increases. In addition, as the temperature increases, the overall uncertainty in force calculation increases. However, the largest differences f_{MTP}–f_{DFT} do not occur for the largest forces, which typically appear in reactions (e.g., bond breaking). With an eye on the computational effort – the simulation time for a level–20 MTP increases ~6-fold, that of a level–22 already ~10-fold over that of level–12 – we decided to obtain results for this study using the level-12 MTP as our MLIP.

3 Results

This study's scope is developing a machine–learning interatomic potential (MLIP) for the simulation of pre-ceramic SiCOH polymers, their pyrolysis, and products. We split our results into two sections: modeling low-temperature dynamics through vibrational spectra and simulating polymer degradation and reactions in the high-temperature range. Throughout this section, we present results for the level–12 MTP only.

3.1 Simulations at low temperature

We first consider vibrational densities of states (vDOS) for models of polydimethyl– and polydiphenylsiloxane (3D rod-packing of PDMS and PDPhS), a model of a–SiO_2:C_f with embedded graphitic carbon (lacking hydrogen), and a large SiCO(:H) structure generated via simulated pyrolysis of PDPhS. For polymeric structures, we look for signatures originating from the Si-O backbone and from substituents (Si-C and C-H). For the structures with free carbon, we separate the carbon atoms into “graphitic carbon”, which we define as C with 3-fold coordination to C, and other C (e.g. interfacial or “disordered”). The vDOS are computed through velocity autocorrelation functions obtained from dynamic simulations at 300 K using VASPKIT.[58] For both methods, MLIP and aiMD simulations, we used an NVT ensemble, a time-step of 0.25 fs, and simulated 20 ps (80,000 steps) to provide a direct comparison. However, in difference to the development and training of the MLIP, the aiMD simulations here apply softer pseudopotentials

For Peer Review

and a cutoff of 280 eV only. For the a–SiO_2:C_f model with 793 atoms, we performed only 10 ps (40,000 steps).

In Figure 2, we compare the results obtained using MLIP and aiMD simulations. We observe remarkable agreement of vibrational states, with the MLIP data closely resembling the DFT results. Significant vibrations – C–H stretching, Si–CH_3 states, O-dominated vibrations of the siloxane backbone, and signatures resembling D- and G-peaks in graphite – are well captured by MTP. To some extent, this could be expected because snapshots of some dynamic simulations were part of the training set. For polydimethylsiloxane, PDMS, we find characteristic C–H localized vibrations at ~3100 cm^{-1}, 1450 cm^{-1}, and 1140 cm^{-1}. In addition, we observe vibrations of the polymer backbone, Si–O vibrations with dominant contribution by O, at 1050 cm^{-1}. Vibrations located within the Si–CH_3 unit appear at 800 cm^{-1}. The split peak at ~ 3100 cm^{-1} observed in DFT is merged into a single distribution of vibrations in MTP for both H and C contributions. A merging of peaks occurs in other instances as well, at ~ 1000 and 350 cm^{-1}. In the case of polydiphenylsiloxane, PDPhS, we find C–H stretching vibrations at ~3100 cm^{-1}, and a set of states between 1280 and 1550 cm^{-1} localized within the phenyl group. The Si–O vibrations of the polymer backbone again appear at ~1050 cm^{-1}. Vibrations originating from the Si–C_6H_5 group are found at 760 cm^{-1}. The participation of Si in these states is much stronger in PDPhS compared to similar states observed at about the same wavenumber in PDMS due to the higher effective mass of the C6H5 group relative to the CH_3 group.

The a–SiO_2:C_f model is particularly helpful in characterizing the vibrational signature of (potentially existing) interfacial Si–C bonds. Note that C atoms in this model are either surrounded by three other C (C-C_3, then called “graphitic”) or bond to one Si and two C, C–SiC_2. The vDOS obtained with the MLIP agrees well with the data obtained using aiMD simulations. Both spectra reveal a clear difference in the vibrational signatures of C-C_3 versus C–SiC_2. This is an essential difference as it refers to the onset and extent of carbon segregation in SiCO ceramics during pyrolysis and annealing.[59] Only C-C_3 shows notable contributions in the range 1350–1600 cm^{-1}. The vDOS obtained by aiMD reflects D– and G-peaks observed for many carbon-rich

For Peer Review

SiCO materials.[30] Interfacial C, with at least one bond to Si, does not provide significant contributions in this range but typically shows up at significantly lower wave numbers, 1100-1300 cm^{-1}. Assuming a localized perspective, this is due to a much weaker/softer C-Si bond at the interface than a C-C bond inside graphite. Vibrations of the SiO_2 host structure appear in the range typical for silica (1100 cm^{-1}). Overall, the agreement of vDOS between MLIP and aiMD (DFT) is consistent and compelling. There are a few differences, typically at very low frequencies, not at least due to limited simulation times and truncated Fourier transformations.

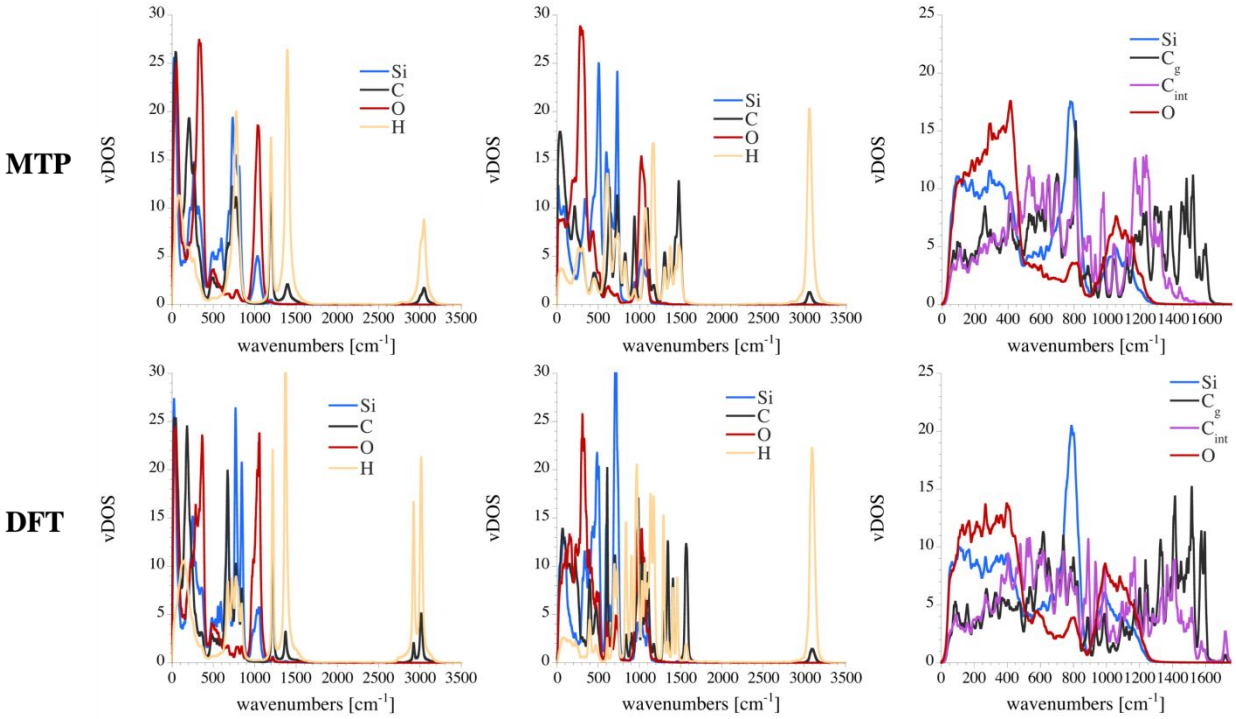

Figure 2: The upper row displays vDOS spectra generated using the MTP for each structure, PDMS, PDPhS, and the model of a–SiO_2:C_f. The lower row shows the corresponding vDOS spectra generated from aiMD simulations. We display partial projections corresponding to each atom type, Si, O, and H, as blue, red, and yellow lines, respectively. For C, we use purple and black lines. The data was generated using VASPKIT.[58]

Provided with some confidence in vibrational results obtained using the MLIP, we turn to the vDOS obtained for a model of pyrolyzed PDPhS. The process of pyrolysis simulations is described in the next section, albeit for a significantly larger model of PDPhS. The model

analyzed here comprises 1,945 atoms and exhibits a sizeable two-dimensional C segregation embedded in a SiCO host matrix; see Figure 3 on the right. Individual graphene sheets are woven into each other, providing connectivity between the layers of the C-segregation. The limited size of the simulation cell (2.8 nm) might impact the particular segregation pattern.[29] The carbon layers also bond to the surrounding host via C–Si bonds. The vDOS presented in Figure 3 shows C–H stretching vibrations at ~3100 cm^{-1}, as some H atoms are still present in this model. The most distinguished signal arises from C–C_3 environments and is found for wavenumbers between 1300 and 1600 cm^{-1} – the region that displays characteristic D– and G–peaks of graphitic segregations in SiCO.[30] A few states related to two-fold coordinated C atoms appear at ~1700 cm^{-1}, indicating that this model is still an "intermediate reaction product". Vibrational states with significant participation of C also appear at ~1200 cm^{-1}. These are due to interfacial C-Si bonds. O-centered states at ~1050 and a signature at ~800 cm^{-1} assigned to vibrational states with Si and C participation indicate the presence of the SiCO host structure.

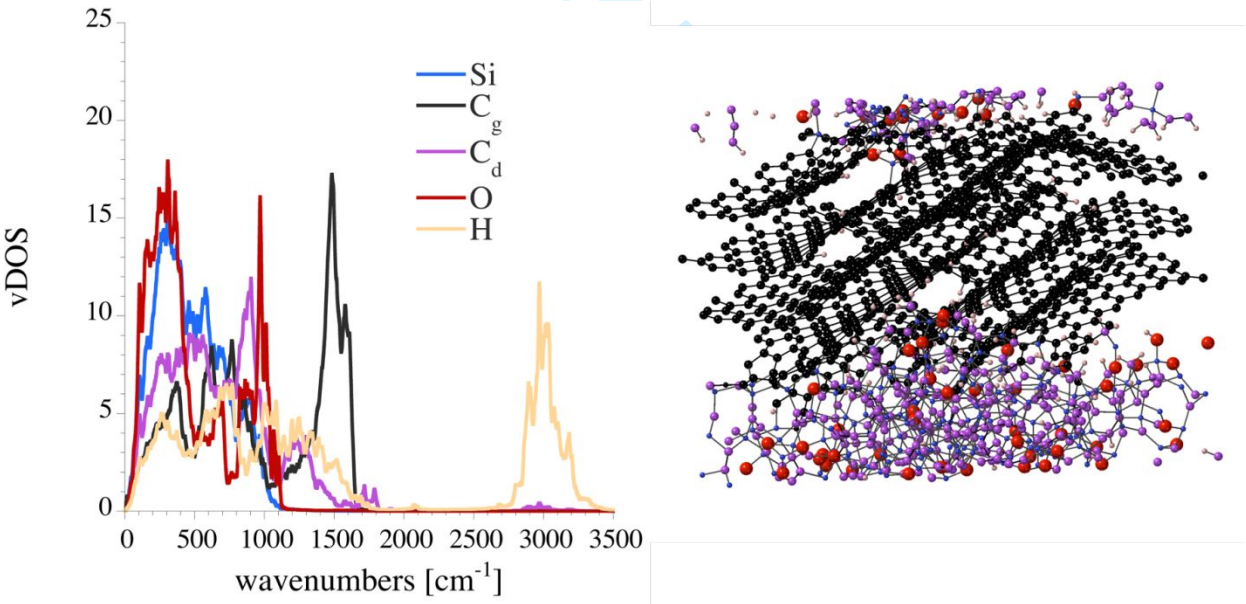

Figure 3: Model of pyrolyzed PDPhS displaying a segregation of "free" carbon. On the left, the vDOS is computed at 300K using classical MD simulation with the MLIP. Lines show partial contribution from Si, C, O, and H. Blue, red, and yellow lines represent Si, O, and H. C atoms with C-C_3 environment are represented black, others magenta. The right shows the structure after pyrolysis. Si, C, O, and H are shown in blue, black/magenta, red, and pink.

Overall, we observe a remarkable alignment of low-temperature vibrational spectra obtained by ab initio (DFT) MD simulations and by MD simulations using the MLIP. Vibrational properties are excellent observables and allow comparison to experimental data. The usefulness of the MLIP becomes apparent, as it computes the vibrational data within a fraction of time compared to the far more expensive aiMD simulation. This way, it becomes possible to model a variety of configurations – in particular, different hypotheses of carbon segregations within SiCO materials[59] – and analyze their respective vibrational pattern. Identifying differences (e.g., the signature of "interfacial C-Si bonds or the onset of developing a "G-peak") will then help to understand the segregation process of "free" carbon. As mentioned before, this outcome of the MLIP generation could be expected because the machine learning process involves just the configurational sampling of localized bonding environments. We remark that framework vibrations with low wavenumbers are still challenging to model properly. These typically involve weaker interaction over larger distances, features not well addressed by our DFT calculations in limited-size models used to build the training set.

3.1 High-temperature simulations

Turning to high-temperature properties, we highlight results of high-temperature simulations of typical polysiloxanes that we performed using the MLIP. We start showing examples of the development of so-called "mixed tetrahedra", SiC_nO_{4-n}–environments that are typical for describing the state of the SiCO glass phase.[60] We built a polydimethylsiloxane (PDMS) model comprising infinite polymer strands in a 3-dimensional rod packing. The structure started with the composition $Si_{2304}C_{4608}O_{2304}H_{13824}$ (= $2304 \cdot SiC_2OH_6$) and a density of 1.0 g/cm^3. After briefly heating, we developed the model at 1400 K and 2000 kbar for 100 ns using a time step Δt=1 fs. During the simulation, the system evolves gaseous molecules, and the polymer undergoes a transformation (pyrolysis) into a ceramic-like state. We remove gaseous species SiH_4, $Si_2O(CH_3)_6$, $Si(CH_3)_3OH$, $Si_2CH_2(CH_3)_6$, $Si(CH_3)_4$, CO_2, CO, CH_4, C_2H_2, C_2H_4, C_2H_6, C_6H_6, CH_2O, O_2, H_2O, CH_3OH, and H_2) from the system every 100 ps using a probabilistic approach inspired by Graham's law. The probability p_{gas} to remove a gas molecule with mass m_{gas} is

For Peer Review

given by $p_{gas} = \sqrt{\frac{m_{H_2}}{m_{gas}}}$. After 100 ns, the composition of the system is $Si_{2290}C_{2352}O_{2284}H_{4780}$ or $Si_{1.0}C_{1.0}O_{1.0}H_{2.1}$. Thus, a lot of hydrogen is still present in the system. Figure 4 shows the progress of SiC_nO_{4-n}–environments during the simulation. The mixed SiC_nO_{4-n}–tetrahedra are labeled by letters following the standard convention of Q, T, D, M, and X for n=0, 1, 2, 3, 4, respectively. Note that the distribution of mixed tetrahedra in a random bond model follows random statistic, with $p(SiC_nO_{4-n}) = \frac{4!}{(4-n)!n!} p_{Si-O}{}^{4-n} p_{Si-C}{}^{n}$. The Si–O and Si–C bond probabilities are computed from the composition $x \cdot SiC + (1-x) \cdot SiO_2$ of the glass phase, $p_{Si-O}=(1-x)/2$ and $p_{Si-C}=1-p_{Si-O}$. The PDMS model starts with only D sites, but significant parts of these soon convert according to the redistribution reaction $2D \rightarrow M + T$. In addition, the pyrolysis reactions form new bonds and create new environments. After 100 ns simulation at 1400 K, we observe a distribution of SiC_nO_{4-n}–tetrahedra with 2.4 (6.2), 25.8 (24.9), 50.1 (37.5), 20.4 (25.1), 1.3 (6.3) %, for n=0,1,2,3,4, respectively, with the values for a perfect random network given in parentheses. With ongoing chemical reactions, the system steadily approaches the "ideal" random network distribution.

In another simulation, we perform the same analysis of the distribution of SiC_nO_{4-n}–tetrahedra during pyrolysis of polymethylhydrosiloxane (PMHS). The simulation parameters were similar to those for PDMS, but we heated the system to 2500 K instead this time. In this simulation, we prevented the removal of CH_4 and H_2O. The evolution of the distribution of SiC_nO_{4-n}–tetrahedra in this system is shown in Figure 4 on the right side. The data fluctuates significantly more in this simulation due to the higher temperatures. The average values computed for snapshots taken between 150–200 ns for the distribution of SiC_nO_{4-n}–tetrahedra are 6.3 (5.6), 26.0 (23.7), 38.6 (37.4), 23.8 (26.3), and 5.3 (6.9) %, for n=0,1,2,3,4, respectively. As before, the values in parentheses are those for a perfect random network. Note that the system is still evolving, and the amounts of SiC_4– and SiO_4–tetrahedra are continuously increasing.

For Peer Review

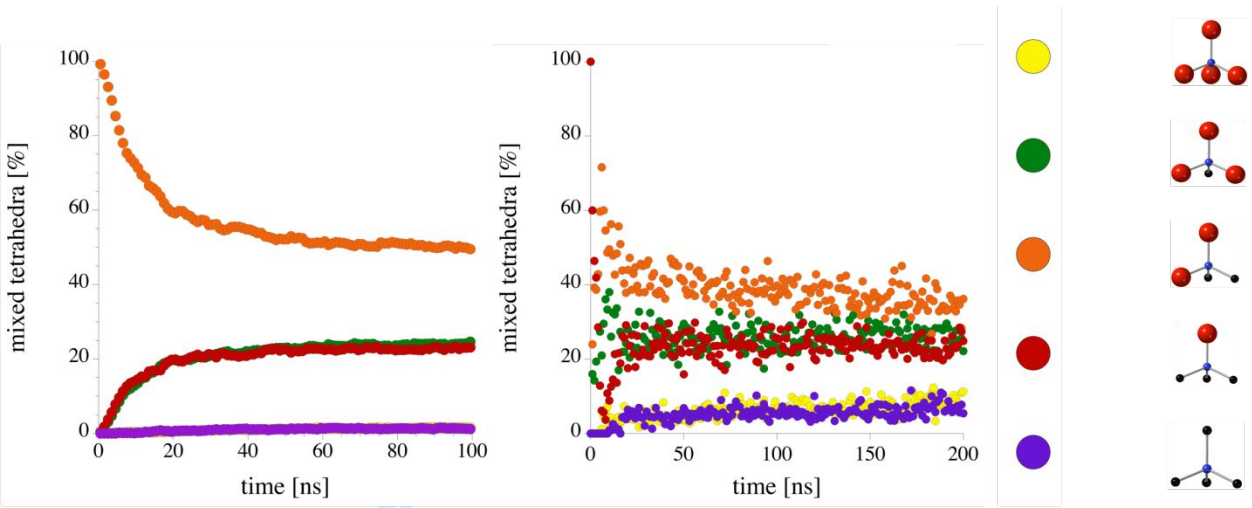

Figure 4: Distributions of SiC_nO_{4-n}–tetrahedra observed during pyrolysis simulation of PDMS and PMHS shown on the left and the right, respectively. The color codes and local configurations of "mixed" SiC_nO_{4-n}–tetrahedra tetrahedra are displayed to the right. Si, C, and O are shown in blue, black, and red.

Moving further to high-temperature pyrolysis simulations, we address a large SiCO system with significant "excess carbon". We built a model of polydiphenylsiloxane (PDPhS), comprising a 3D rod packing of 8-mers, with composition $Si_{41472}C_{414720}O_{41472}H_{497664}$ (= 41472 · $[SiO(C_5H_6)_2]$). Hence, the initial model includes about 1 million atoms. After increasing the temperature, we simulated 2500 K under constant pressure (8000 kbar) for 10 nanoseconds. We removed gaseous species every 10 ps using the "Graham-inspired" method described above. After 10 ns simulation time, the system has the composition $Si_{41472}C_{367124}O_{9114}H_{57248}$ or $SiC_{8.9}O_{0.2}H_{1.4}$. The size of the corresponding simulation box is 17.9 nm. The model after 10 ns comprises about 292,864 C atoms with three or two bonds to other C. We selected those as the "free" carbon phase and show them in Figure 5.

For Peer Review

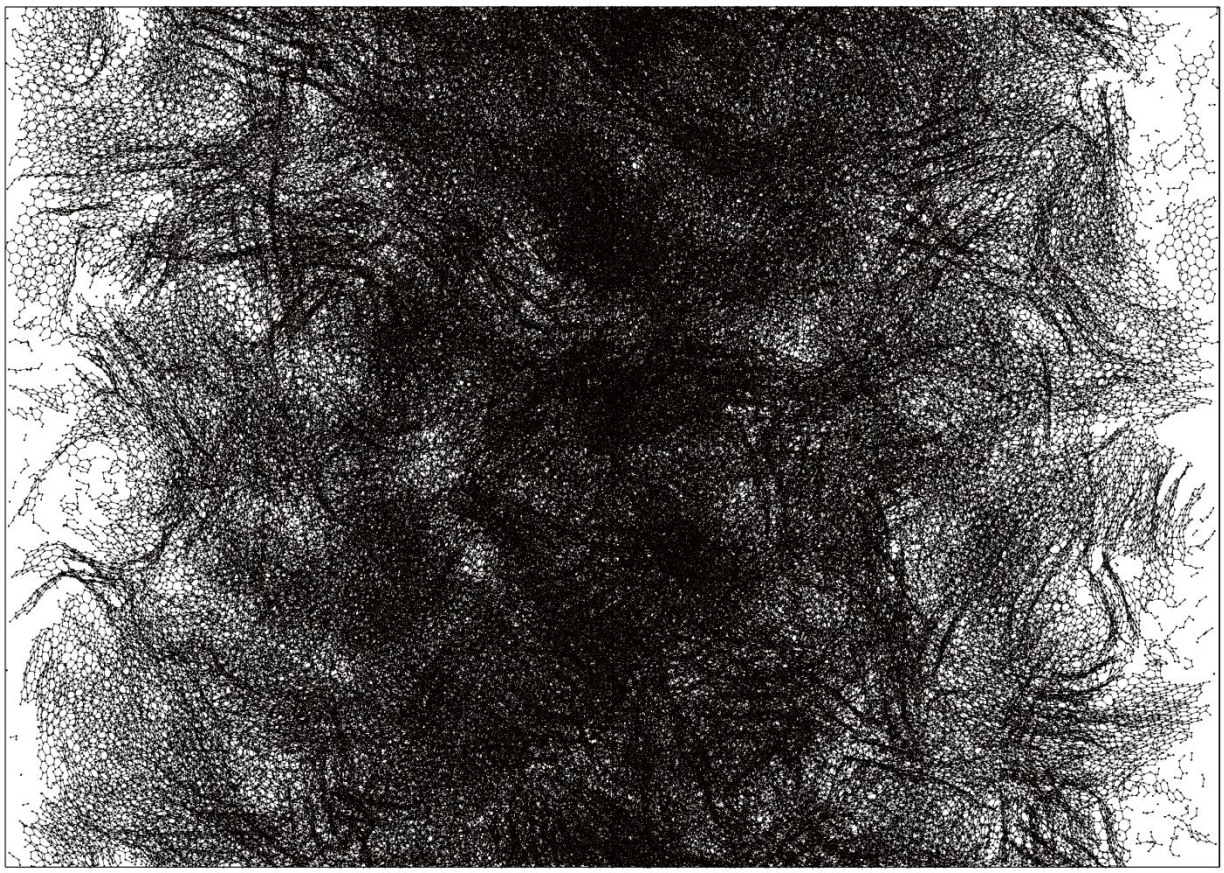

Figure 5: The "Free" carbon phase is observed in a pyrolysis model of PDPhS after 10 ns at 2500 K. Only those C atoms of the structure at least two-fold coordinated to other C atoms are shown (292,864 C). Other C atoms and all Si, O, and H atoms are omitted. The cubic simulation box (a ≈ 17.9 nm) is rotated by 45° to facilitate the view along the "thin" edges, where the background is small enough to decipher individual sheets and stacked layers.

The model allows us to identify individual graphene layers that formed during pyrolysis. Most layers display curvature; in some cases, layers form small tubes. Stacked layers also occur, with a typical distance between layers of 3.2–3.9 nm. Note that there is still a small amount of SiCO and some H dispersed throughout the structure, which is not shown in the structure.

Our third example highlights detailed local chemical reactions found on trajectories generated during MD simulations using the MLIP. We isolated a process in which methane gas is formed, leaving behind a bridging Si-CH_2-Si, as shown in Figure 6. We observed this reaction in a classical MD NVT simulation of a model of PDMS at 1400K. The process itself begins with the

formation of 3-coordinated Si. This reactive Si then bridges to its second-nearest neighbor Si via a methyl group, forming a short-lived Si-CH_3-Si intermediate. The extra H migrates further and bonds with a methyl group, forming CH_4. The 3-coordinated Si left behind eventually finds a fourth partner in an adjacent Si's reactive CH_2. The initial steps, including the CH_4 abstraction, of this and similar processes happen within ~100 fs. In contrast, the final step of saturating the Si often takes one or two orders of magnitude longer to complete.

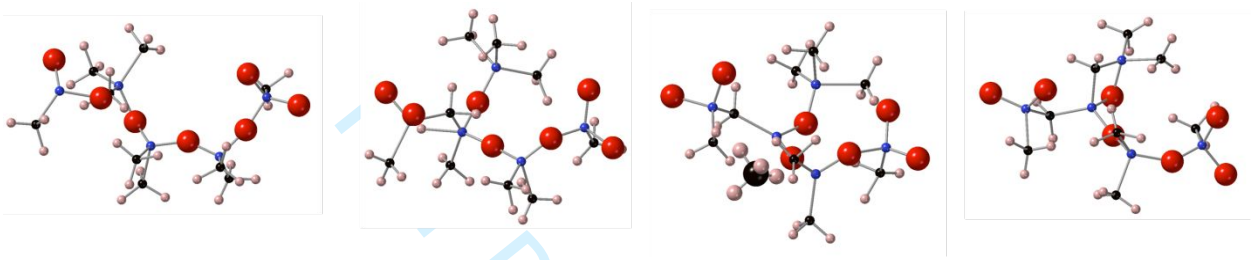

Figure 6: Still images of the trajectory of a process generating methane, CH_4. Atoms irrelevant to the reaction are omitted in this display. Initially, a CH_3 migrates from one Si to another, creating a 3-coordinated Si as an intermediate. The Si quickly finds an adjacent CH_3, forming a Si-CH_2-Si bridge and a very long Si…H interaction. This H joins a methyl group on the Si, forming CH_4 (displayed by a fat C atom). The 3-coordinated Si left behind eventually forms another Si-CH_2-Si linkage. Si, C, O, and H are shown in blue, black, red, and pink, respectively.

For the last demonstration of detailed high-temperature reactions, we turn to a specific mode of reorganization that is essential during the pyrolysis of polysiloxanes: the integration of carbon atoms originating from organic side groups into the siloxane polymer backbone. The process is similar to the Yajima process, which converts a polysilane into a polycarbosilane by migrating one of the methyl substituents into the polymer chain.[61] This migration is known as Kumada rearrangement and was first characterized for simple silane molecules such as hexamethyldisilane.[47] In polysiloxanes, the corresponding rearrangement inserts C from an aliphatic ligand on Si, typically a CH_3 group, into the Si–O–Si polymer backbone. We refer to this process as "Kumada-like" due to its resemblance with the original Kumada rearrangement. We observed this rearrangement multiple times during extensive aiMD simulations of PDMS and PMHS at elevated temperatures and could extract isolated processes without overlapping

secondary reactions. As mentioned earlier, we included selected configurations from the trajectory in our training set of the MLIP. Performing dynamic simulations of PDMS at elevated temperatures using the MLIP, we then observe several instances of a migration of a methylene group into the siloxane backbone. One such process is shown by individual snapshots of the trajectory in Figure 6. The process occurs over the course of several 100fs (here at 2500 K). A 5-coordinated Si and a 5-coordinated C are observed as short-living intermediates during the transition.

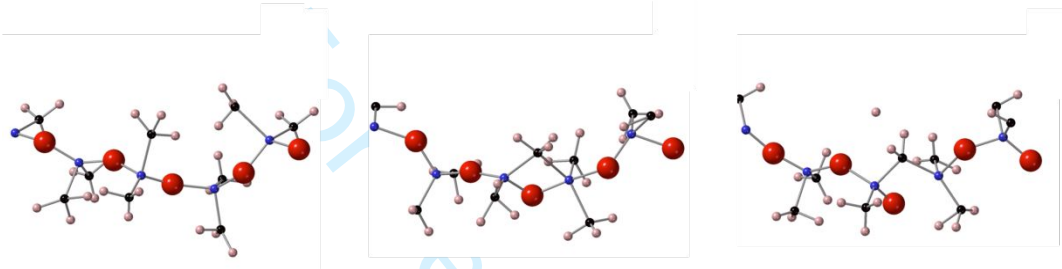

Figure 7: Snapshots (still images) along the trajectory of a Kumada-like rearrangement in polydimethylsiloxane. Atoms irrelevant to the reaction are omitted in this display. The methyl group at the center of each individual still image migrates from one Si to form a five-coordinated intermediate with the adjacent Si. Note that the second Si transformed its local environment from SiC_2O_2 to SiC_3O, hence D -> T, while the other Si retained its environment. Si, C, O, and H are shown in blue, black, red, and pink, respectively.

4 Discussion

The results demonstrate that the machine–learning interatomic potentials (MLIPs) that we developed are capable of dynamic simulations of Si-C-O-H compounds. Such simulations target structure and low-temperature vibrational properties but also include detailed chemical reactions occurring at high temperatures. The MLIPs were generated using MTPs and fitted to energies, forces, and stresses of DFT data. Additional active-learning techniques further augmented the training set “on the fly” and improved the MLIPs. Due to the diversity of the training data, the potential has a large applicability range. It can describe the formation of SiCO compounds and their properties in a large temperature and pressure range.

We demonstrate that the MLIP successfully reproduces vibrational properties of SiCOH obtained from aiMD simulations. This motivates us to appraise the quality of the MLIP simulations as having a "DFT-like" quality. With fidelity in the method established, it is possible to investigate significantly larger models that comprise structural features that cannot be captured in small models and computed using DFT. For example, detailed investigations are required of the genesis of carbon segregations in SiCO ceramics and of the interface between segregated carbon and the surrounding SiCO host matrix.[59] Such studies shall work out observables that can be measured in experiments, and a comparison of computational and experimental data will discriminate between different models that have been proposed.

The MLIP also simulates the conversion of polymers into SiCO ceramics at high temperatures. The distribution of tetrahedra aligns well with the expectations of the SiCO glass phase that have been established in many experimental studies. We also demonstrate a simulation starting with 1,000,000 atoms and developing the system for 10 ns. This large-scale simulation features a model in a simulation box with box length a ≈ 17.9 nm and volume of V ≈ 6400 nm^3. While this is still a microscopic model, it will allow studying the segregation and formation of different phases in SiCO with high accuracy at unprecedented length and time scales.

Compared to aiMD simulations, the MLIPs are significantly faster and, in addition, allow much larger length scales to be addressed. Compared to reactive simulations using ReaxFF with the parameters we developed earlier,[28] we estimate that the MLIP is about 40 times faster per time step of the simulation. Since ReaxFF requires careful time step adjustment for both the integration of the equations of motion and the charge equilibration, we find the overall speed-up even higher.

The provided MLIPs are not perfect and will need to be developed further. There are fundamental challenges to MLIPs, for example the mobility of charges or spins, that impact all reactive systems.[39] A noticeable imperfection of the MLIPs presented here is a low reactivity of CH_4 and H_2O molecules once these are generated. This behavior becomes visible only in more

For Peer Review

extended simulations and if gaseous molecules are removed. Eventually, the molecules will react even with the MLIP. A comparison to aiMD simulation that we performed for up to 1 ns, however, indicates too slow kinetics of reactions of these molecules. Adding selected configurations of reaction trajectories obtained from additional aiMD simulation will help to remedy this issue in the future. Another imperfection we observed is a high abundance in C-Si_3– environments in the SiCO glass phase after the final optimization of a model. Subsequent spin-polarized DFT optimization of such geometries yields a high population of unpaired spins, indicating high magnetization. We note that all the observed imperfections became visible only after extended MD simulations, which is why current active-learning strategies cannot address such situations "on the fly". Despite these imperfections, the MLIPs here deliver simulations of polysiloxanes and SiCOH ceramics with unprecedented quality and form a tool to advance understanding of the chemical and structural development in such complex systems.

4 Summary

In this contribution, we show the development of Machine–Learning Interatomic Potentials (MLIPs) for simulations of polysiloxanes and SiCO ceramics based on Moment-Tensor-Potentials (MTPs). Taking advantage of our extensive library of SiCOH configurations, we trained the MLIPs to polymer structures, crystalline and amorphous SiCOH structures, and included trajectories of ab-initio molecular dynamic (aiMD) simulations of SiCOH structures at elevated temperatures. Beyond passive training to energies, forces, and stresses, we applied active-learning strategies and implemented further hybrid learning to improve the MLIPs. The results demonstrate that the MLPs simulate low-temperature properties of polysiloxanes and SiCOH ceramics with "DFT-like" quality. Beyond properties close to a local minimum configuration, we show examples of simulations of the polymer-to-ceramic transformation. Individual chemical reactions become visible and can be studied in detail, and million-atom simulations extending over several nanoseconds are feasible. The structural development of mixed tetrahedra in SiCO ceramics and the precipitation of nanometer-sized graphitic

For Peer Review

segregations in C-rich SiCO systems align with experimental observations, demonstrating a high fidelity of the MLIPs. We have also identified some imperfections of the MLIPs that can be remedied in future systematic improvement. Overall, the MLIPs deliver "DFT-like" quality in multi-million atom simulations of SiCOH for modeling nanoscale structures and pyrolysis simulations extending for several nanoseconds.

Acknowledgment

This work used Expanse at San Diego Supercomputer Center (SDSC) and Stampede2 and Lonestar6 at Texas Advanced Computing Center (TACC) through allocation DMR190103 from the Advanced Cyberinfrastructure Coordination Ecosystem: Services & Support (ACCESS) program, which is supported by National Science Foundation grants #2138259, #2138286, #2138307, #2137603, and #2138296. Significant contributions of earlier results were obtained at the same systems through allocation DMR190103 from the Extreme Science and Engineering Discovery Environment (XSEDE), which was supported by National Science Foundation grant number #1548562. Additional computational work was made possible by the High-Performance Computing facilities at UTA. This work was partially supported by the National Science Foundation (NSF) through award #1743701.

For Peer Review

References

1. Nguyen, M. D.; Bang, J. W.; Bin, A. S.; Kim, S.-R.; Kim, Y.; Hwang, K. H.; Pham, V.-H.; Kwon, W.-T., Novel Polymer-Derived Ceramic Environmental Barrier Coating System for Carbon Steel in Oxidizing Environments. *Journal of the European Ceramic Society* **2017**, *37*, 2001-2010.
2. Stabler, C.; Ionescu, E.; Graczyk-Zajac, M.; Gonzalo-Juan, I.; Riedel, R., Silicon Oxycarbide Glasses and Glass-Ceramics: "All-Rounder" Materials for Advanced Structural and Functional Applications. *Journal of the American Ceramic Society* **2018**, *101*, 4817-4856.
3. Liu, C.; Pan, R.; Hong, C.; Zhang, X.; Han, W.; Han, J.; Du, S., Effects of Zr on the Precursor Architecture and High-Temperature Nanostructure Evolution of Sioc Polymer-Derived Ceramics. *Journal of the European Ceramic Society* **2016**, *36*, 395-402.
4. Fukui, H.; Ohsuka, H.; Hino, T.; Kanamura, K., A Si−O−C Composite Anode: High Capability and Proposed Mechanism of Lithium Storage Associated with Microstructural Characteristics. *ACS Applied Materials & Interfaces* **2010**, *2*, 998-1008.
5. Lee, J.; Jang, W.; Kim, H.; Shin, S.; Kweon, Y.; Lee, K.; Jeon, H., Characteristics of Low-K Sioc Films Deposited Via Atomic Layer Deposition. *Thin Solid Films* **2018**, *645*, 334-339.
6. Vakifahmetoglu, C.; Zeydanli, D.; Innocentini, M. D. d. M.; Ribeiro, F. d. S.; Lasso, P. R. O.; Soraru, G. D., Gradient-Hierarchic-Aligned Porosity Sioc Ceramics. *Scientific Reports* **2017**, *7*, 41049.
7. Merida, J.; Colomer, M. T.; Rubio, F.; Mazo, M. A., Highly Porous Carbon Materials Derived from Silicon Oxycarbides and Effect of the Pyrolysis Temperature on Their Electrochemical Response. *Int J Mol Sci* **2023**, *24*.
8. Tamayo, A.; Mazo, M. A.; Ruiz-Caro, R.; Martín-Illana, A.; Bedoya, L. M.; Veiga-Ochoa, M. D.; Rubio, J., Mesoporous Silicon Oxycarbide Materials for Controlled Drug Delivery Systems. *Chemical Engineering Journal* **2015**, *280*, 165-174.
9. Soraru, G.; Pederiva, L.; Latournerie, J.; Raj, R., Pyrolysis Kinetics for the Conversion of a Polymer into an Amorphous Silicon Oxycarbide Ceramic. *Journal of the American Ceramic Society* **2004**, *85*, 2181-2187.
10. Jana, P.; Santoliquido, O.; Ortona, A.; Colombo, P.; Sorarù, G. D., Polymer-Derived Sicn Cellular Structures from Replica of 3d Printed Lattices. *JOURNAL OF THE AMERICAN CERAMIC SOCIETY* **2018**, *101*, 2732-2738.
11. Kemp, J. W.; Reed, J. L.; Compton, B. G., Size Effects in 3d-Printed Polymer-Derived, Zirconium Diboride-Reinforced Ceramic Composites. *JOURNAL OF THE AMERICAN CERAMIC SOCIETY* **2024**, *107*, 1557-1570.
12. Monte, F. A. D.; Awad, K. R.; Ahuja, N.; Kim, H. K. W.; Aswath, P.; Brotto, M.; Varanasi, V. G., Amorphous Silicon Oxynitrophosphide-Coated Implants Boost Angiogenic Activity of Endothelial Cells. *Tissue Eng Part A* **2020**, *26*, 15-27.

For Peer Review

13. Bai, W. R.; Widgeon, S.; Sen, S., Structure and Topological Characteristics of Amorphous Silicon Oxycarbide Networks: Results from Reverse Monte Carlo Simulations. *JOURNAL OF NON-CRYSTALLINE SOLIDS* **2014**, *386*, 29-33.
14. Widgeon, S. J.; Sen, S.; Mera, G.; Ionescu, E.; Riedel, R.; Navrotsky, A., 29si and 13c Solid-State Nmr Spectroscopic Study of Nanometer-Scale Structure and Mass Fractal Characteristics of Amorphous Polymer Derived Silicon Oxycarbide Ceramics. *Chemistry of Materials* **2010**, *22*, 6221-6228.
15. Saha, A.; Raj, R.; Williamson, D. L., A Model for the Nanodomains in Polymer-Derived Sico. *Journal of the American Ceramic Society* **2006**, *89*, 2188-2195.
16. Kroll, P., Modeling the 'Free Carbon' Phase in Amorphous Silicon Oxycarbide. *JOURNAL OF NON-CRYSTALLINE SOLIDS* **2005**, *351*, 1121-1126.
17. Kleebe, H.-J.; Turquat, C.; Sorarù, G. D., Phase Separation in an Sico Glass Studied by Transmission Electron Microscopy and Electron Energy-Loss Spectroscopy. *Journal of the American Ceramic Society* **2001**, *84*, 1073-1080.
18. Mazo, M. A.; Soriano, D.; Rubio, J., Mechanical Response of Silicon Oxycarbide Materials Processed by Spark Plasma Sintering. *Ceramics International* **2023**, *49*, 12866-12875.
19. Colombo, P.; Mera, G.; Riedel, R.; Sorarù, G. D., Polymer-Derived Ceramics: 40 Years of Research and Innovation in Advanced Ceramics. *Journal of the American Ceramic Society* **2010**, *93*, 1805-1837.
20. Riedel, R.; Mera, G.; Hauser, R.; Klonczynski, A., Silicon-Based Polymer-Derived Ceramics: Synthesis Properties and Applications-a Review Dedicated to Prof. Dr. Fritz Aldinger on the Occasion of His 65th Birthday. *Journal of the Ceramic Society of Japan (日本セラミックス協会学術論文誌)* **2006**, *114*, 425-444.
21. Kroll, P., Modelling and Simulation of Amorphous Silicon Oxycarbide. *JOURNAL OF MATERIALS CHEMISTRY* **2003**, *13*, 1657-1668.
22. Kroll, P., Searching Insight into the Atomistic Structure of Sico Ceramics. *JOURNAL OF MATERIALS CHEMISTRY* **2010**, *20*, 10528-10534.
23. Bodiford, N. Crystalline ~~Sico~~SiCO: Implication on Structure and Thermochemistry of Ternary Silicon Oxycarbide Ceramics. Thesis; The University of Texas at Arlington; **2014**.
24. Nimmo, J. P.; Kroll, P., First-Principles Calculations and Analysis of Si-29 Nuclear Magnetic Resonance Chemical Shifts in Silicon Oxycarbide Ceramics. *JOURNAL OF PHYSICAL CHEMISTRY C* **2014**, *118*, 29952-29961.
25. Leimeroth, N.; Rohrer, J.; Albe, K., Structure-Property Relations of Silicon Oxycarbides Studied Using a Machine Learning Interatomic Potential. *Journal of the American Ceramic Society ~~arXiv preprint arXiv:2403.10154~~* **2024**. DOI10.1111/jace.19932.
26. Gao, H. F.; Wang, H. J.; Zhao, Z. H.; Niu, M.; Su, L.; Wei, Y., Reactive Dynamics Simulation Study on the Pyrolysis of Polymer Precursors to Generate Amorphous Silicon Oxycarbide Structures. *JOURNAL OF PHYSICAL CHEMISTRY C* **2018**, *122*, 5767-5773.
27. Ding, H. P.; Demkowicz, M. J., Hydrogen Reverses the Clustering Tendency of Carbon in Amorphous Silicon Oxycarbide. *SCIENTIFIC REPORTS* **2015**, *5*.

For Peer Review

28. Ponomarev, I.; van Duin, A. C. T.; Kroll, P., Reactive Force Field for Simulations of the Pyrolysis of Polysiloxanes into Silicon Oxycarbide Ceramics. *The Journal of Physical Chemistry C* **2019**, *123*, 16804-16812.
29. Haseen, S.; Kroll, P., Analyzing the Effect of Composition, Density, and the Morphology of the "Free" Carbon Phase on Elastic Moduli in Silicon Oxycarbide Ceramics. *Journal of the European Ceramic Society* **2023**, *43*, 1432-1441.
30. Mera, G.; Kroll, P.; Ponomarev, I.; Chen, J.; Morita, K.; Liesegang, M.; Ionescu, E.; Navrotsky, A., Metal-Catalyst-Free Access to Multiwalled Carbon Nanotubes/Silica Nanocomposites (Mwcnt/Sio2) from a Single-Source Precursor. *Dalton Transactions* **2019**, *48*, 11018-11033.
31. Bartók, A. P.; Payne, M. C.; Kondor, R.; Csányi, G., Gaussian Approximation Potentials: The Accuracy of Quantum Mechanics, without the Electrons. *Physical Review Letters* **2010**, *104*, 136403.
32. Bartók, A. P.; Kondor, R.; Csányi, G., On Representing Chemical Environments. *Physical Review B* **2013**, *87*, 184115.
33. Behler, J.; Parrinello, M., Generalized Neural-Network Representation of High-Dimensional Potential-Energy Surfaces. *Physical Review Letters* **2007**, *98*, 146401.
34. Drautz, R., Atomic Cluster Expansion for Accurate and Transferable Interatomic Potentials. *Physical Review B* **2019**, *99*, 014104.
35. Dusson, G.; Bachmayr, M.; Csányi, G.; Drautz, R.; Etter, S.; van der Oord, C.; Ortner, C., Atomic Cluster Expansion: Completeness, Efficiency and Stability. *Journal of Computational Physics* **2022**, *454*, 110946.
36. Thompson, A. P.; Swiler, L. P.; Trott, C. R.; Foiles, S. M.; Tucker, G. J., Spectral Neighbor Analysis Method for Automated Generation of Quantum-Accurate Interatomic Potentials. *Journal of Computational Physics* **2015**, *285*, 316-330.
37. Schütt, K. T.; Sauceda, H. E.; Kindermans, P. J.; Tkatchenko, A.; Müller, K. R., Schnet – a Deep Learning Architecture for Molecules and Materials. *The Journal of Chemical Physics* **2018**, *148*, 241722.
38. Batzner, S.; Musaelian, A.; Sun, L.; Geiger, M.; Mailoa, J. P.; Kornbluth, M.; Molinari, N.; Smidt, T. E.; Kozinsky, B., E(3)-Equivariant Graph Neural Networks for Data-Efficient and Accurate Interatomic Potentials. *Nature Communications* **2022**, *13*, 2453.
39. Behler, J.; Csányi, G., Machine Learning Potentials for Extended Systems: A Perspective. *The European Physical Journal B* **2021**, *94*, 142.
40. Shapeev, A. V., Moment Tensor Potentials: A Class of Systematically Improvable Interatomic Potentials. *Multiscale Modeling & Simulation* **2016**, *14*, 1153-1173.
41. Novikov, I. S.; Shapeev, A. V., Improving Accuracy of Interatomic Potentials: More Physics or More Data? A Case Study of Silica. *Materials Today Communications* **2019**, *18*, 74-80.
42. Novoselov, II; Yanilkin, A. V.; Shapeev, A. V.; Podryabinkin, E. V., Moment Tensor Potentials as a Promising Tool to Study Diffusion Processes. *COMPUTATIONAL MATERIALS SCIENCE* **2019**, *164*, 46-56.

For Peer Review

43. Zongo, K.; Sun, H.; Ouellet-Plamondon, C. M.; B'eland, L. K. In *A Unified Moment Tensor Potential for Silicon, Oxygen, and Silica*, 2023.
44. Podryabinkin, E. V.; Kvashnin, A. G.; Asgarpour, M.; Maslenikov, I. I.; Ovsyannikov, D. A.; Sorokin, P. B.; Popov, M. Y.; Shapeev, A. V., Nanohardness from First Principles with Active Learning on Atomic Environments. *Journal of Chemical Theory and Computation* **2022**, *18*, 1109-1121.
45. Novikov, I. S.; Gubaev, K.; Podryabinkin, E. V.; Shapeev, A. V., The Mlip Package: Moment Tensor Potentials with Mpi and Active Learning. *Machine Learning: Science and Technology* **2021**, *2*, 025002.
46. Podryabinkin, E.; Garifullin, K.; Shapeev, A.; Novikov, I., Mlip-3: Active Learning on Atomic Environments with Moment Tensor Potentials. *The Journal of Chemical Physics* **2023**, *159*, 084112.
47. Shiina, K.; Kumada, M., Notes - Thermal Rearrangement of Hexamethyldisilane to Trimethyl(Dimethylsilylmethyl)Silane. *The Journal of Organic Chemistry* **1958**, *23*, 139-139.
48. Kresse, G.; Hafner, J., Ab Initio Molecular Dynamics for Liquid Metals. *Physical Review B* **1993**, *47*, 558-561.
49. Kresse, G.; Furthmüller, J., Efficient Iterative Schemes for Ab Initio Total-Energy Calculations Using a Plane-Wave Basis Set. *Physical Review B* **1996**, *54*, 11169-11186.
50. Kresse, G.; Furthmüller, J., Efficiency of Ab-Initio Total Energy Calculations for Metals and Semiconductors Using a Plane-Wave Basis Set. *Computational Materials Science* **1996**, *6*, 15-50.
51. Blöchl, P. E., Projector Augmented-Wave Method. *Physical Review B* **1994**, *50*, 17953-17979.
52. Kresse, G.; Joubert, D., From Ultrasoft Pseudopotentials to the Projector Augmented-Wave Method. *Physical Review B* **1999**, *59*, 1758-1775.
53. Perdew, J. P.; Burke, K.; Ernzerhof, M., Generalized Gradient Approximation Made Simple. *Physical Review Letters* **1996**, *77*, 3865-3868.
54. Perdew, J. P.; Burke, K.; Ernzerhof, M., Generalized Gradient Approximation Made Simple [Phys. Rev. Lett. 77, 3865 (1996)]. *Physical Review Letters* **1997**, *78*, 1396-1396.
55. Kim, H.; Choi, J.-M.; Goddard, W. A., III, Universal Correction of Density Functional Theory to Include London Dispersion (up to Lr, Element 103). *The Journal of Physical Chemistry Letters* **2012**, *3*, 360-363.
56. Thompson, A. P., et al., Lammps - a Flexible Simulation Tool for Particle-Based Materials Modeling at the Atomic, Meso, and Continuum Scales. *Computer Physics Communications* **2022**, *271*, 108171.
57. Morrow, J. D.; Gardner, J. L. A.; Deringer, V. L., How to Validate Machine-Learned Interatomic Potentials. *The Journal of Chemical Physics* **2023**, *158*, 121501.
58. Wang, V.; Xu, N.; Liu, J.-C.; Tang, G.; Geng, W.-T., Vaspkit: A User-Friendly Interface Facilitating High-Throughput Computing and Analysis Using Vasp Code. *Computer Physics Communications* **2021**, *267*, 108033.

For Peer Review

59. Wen, Q.; Yu, Z.; Riedel, R., The Fate and Role of in Situ Formed Carbon in Polymer-Derived Ceramics. *Progress in Materials Science* **2020**, *109*, 100623.
60. Zhang, H.; Pantano, C. G., Synthesis and Characterization of Silicon Oxycarbide Glasses. *JOURNAL OF THE AMERICAN CERAMIC SOCIETY* **1990**, *73*, 958-963.
61. Murase, H.; Kawasaki, S.; Kitaoka, T.; Furukawa, J.; Ueda, H.; Nishimura, H.; Yamada, K., Effects of Polysilane-Coating on Interface of Electrofusion Joints for Maintaining Strength. *Materials Sciences and Applications* **2015**, *06*, 322-331.

For Peer Review

Machine Learning Interatomic Potentials for Pyrolysis of Polysiloxanes and Properties of SiCO Ceramics

Mitchell Falgoust and Peter Kroll*

Department of Chemistry and Biochemistry, The University of Texas at Arlington,
700 Planetarium Place, Arlington, Texas 76019, United States.

* Corresponding authors: pkroll@uta.edu

For Peer Review

Abstract

We present Machine–Learning Interatomic Potentials (MLIPs) for simulations of Si-C-O-H compounds. The MLIPs are constructed from Moment-Tensor-Potentials (MTPs) and were trained to a library of configurations that included polysiloxane structures, hypothetical crystalline and amorphous SiCOH structures, and trajectories of Si-C-O-H systems obtained via ab-initio molecular dynamic (aiMD) simulations at elevated temperatures. Passive, active, and hybrid learning strategies were implemented to develop the MLIPs.

The MLIPs reproduce vibrational properties of polymers and SiCOH structures obtained from aiMD simulations, thus providing a tool to identify chemical units and distinct structural characteristics through their vibrational properties. Simulations of the polymer-to-ceramic transformation show the development of mixed tetrahedra in SiCO ceramics and align with experimental observations. Million-atom simulations for several nanoseconds highlight the precipitation of graphitic nanosheets from a carbon-rich SiCO precursor. Atomistic simulations with the MLIPs deliver details of chemical reaction mechanisms during the pyrolysis of polysiloxanes, including methane abstraction and Kumada-like rearrangements that transform the siloxane backbone. While the MLIPs still leave room for systematic improvement, they deliver simulations with “DFT-like” quality at low and high temperatures.

1 Introduction

Polymer-derived silicon oxycarbide (SiCO) ceramics are known for high thermal and chemical stability, biocompatibility, intriguing electrical properties at extreme conditions,[1-3] and potential use as anode material for Li^+ or Na^+ storage.[4-5] Porous SiCO can be selectively synthesized with micro-, meso-, and macroporosity and is a membrane material for separations or a vehicle for drug delivery systems.[6-8] The polymer-to-ceramics route is a versatile and robust approach,[9] and many polysiloxanes are applied as SiCOH precursors for polymer-derived ceramics (PDCs). New trends in processing and applications include additive manufacturing and tooth and bone implants.[10-12]

The thermal conversion of a pre-ceramic siloxane polymer into a SiCO ceramic generates various intermediate states, and the temperature and environment atmosphere chosen during processing impact the composition and morphology of the resulting material. Pyrolysis typically occurs between 400 and 1000°C and yields an amorphous SiCO ceramic[2] that comprises a glassy network in which additional "excess" or "free" carbon is embedded. The SiCO glass comprises corner-sharing SiC_nO_{4-n}–tetrahedra (n=1–4), so-called "mixed tetrahedra".[13-14] The "free" carbon phase of SiCO is the source of many of the material's functional properties. Determining the carbonaceous structure in amorphous SiCO and its interface to the surrounding glassy SiCO host is challenging, and various hypotheses have been formulated.[14-16] Further annealing of amorphous SiCO at 1200°C and higher temperatures induces a phase separation of glassy SiCO into SiC and SiO_2.[17] Above ~1350˚C, carbothermal reduction transforms "free" carbon and SiO_2 to SiC, releasing CO.[18] Several excellent reviews address the synthesis, characterization, and properties of SiCO ceramics.[2, 14-15, 19-20]

Over the last two decades, modeling and simulation of SiCO materials addressed structure, enthalpy of formation, and some physical and mechanical properties. [21 16, 22-25] Computational studies of chemical reactions during pyrolysis are a recent topic.[26-28] Constant challenges in these simulations are model size, simulation length, and accuracy of the method

For Peer Review

used. Focusing on SiCO simulations, accurate quantum chemical simulations are limited to a few hundred atoms simulated for not much more than a nanosecond. Empirical interatomic potentials such as the Tersoff potential trade in accuracy for speed, enabling simulations of millions of atoms and extending simulations over microseconds. The reactive force-field (ReaxFF)[28-30] approach is located between these antipodes and promises to deliver accurate descriptions of chemical reactions with the speed of an empirical potential. Each method has its range of applicability, and with time moving on, the range and maximum size will be pushed forward.

Recently, so-called machine–learning interatomic potentials (MLIPs) have proven to be an effective new tool that bridges the gap between accurate quantum chemical and empirical potential simulations. Various approaches to construct MLIPs have been presented in the literature under acronyms such as GAP, SOAP, NNP, GNN, ACE, SNAP, and SchNet – by no means an exhaustive list.[31-38] Characteristic of these MLIPs is a representation of chemical interactions by mathematical descriptors of arbitrary complexity.[39] The ML approaches are usually referred to as "non-parametric" in the sense that when building an MLIP, the focus is on optimizing an objective function rather than involving traditional parameters of bonding and interaction. In this work, we develop MLIPs based on Moment Tensor Potentials (MTPs) introduced by Shapeev.[40] MTPs comprise two-body interactions represented by rotationally and translationally invariant polynomials within a predefined cutoff distance. Three- and multi-body interactions are stored in moments. Increasing the number of basis functions, the number of outer products, or the cutoff distance are paths to improve systematically the accuracy of the MLIP.[40] The parameters of the model are fitted to energies, forces, and stresses – that we computed using density-functional theory (DFT) – for a variety of configurations.

Working with the MTP approach to MLIPs, our first goal of this contribution is to provide a high-fidelity tool to model low-temperature properties of SiCO materials, including elastic and plastic deformations or vibrational signatures of phase segregations. This endeavor succeeds, as the process involves only the configurational sampling of localized bonding environments. Our second goal is more far-reaching: we aim to simulate chemical reactions as

For Peer Review

they occur during the pyrolysis of polysiloxanes. Anticipating our results, we obtain new MLIPs suitable to study distinct reaction mechanisms, including the details of carbon migration into the siloxane backbone. The MLIP is fast enough to perform large–scale (1,000,000 atoms) conversions for several nanoseconds with local accuracy resembling DFT simulations.

2 Computational Method

With our goal to develop machine-learning interatomic potentials (MLIPs) for simulations of structure, low-temperature properties, and high-temperature reactivity of polymers comprising the elements Si, C, O, and H, we use the moment tensor potentials (MTPs) developed by Shapeev.[40] This particular approach has been used successfully to describe structural properties of α-SiO_2, diffusion coefficients for Si, and nano-hardness in large SiC models.[41-44] Consequently, MTPs should also be suitable for simulations of SiCO materials and SiCOH pre-ceramic polymers. A detailed description of the formalisms of the MTP representation can be found elsewhere.[40, 45-46]

To obtain the parameters of MTPs, we perform machine learning (linear regression) using an extensive library of DFT configurations with associated energies, forces, and stresses. The training data is provided to the MLIP-2 software[45] that performs the machine learning. The objective function addresses the difference between target (DFT) and computed (MTP) energies, forces, and stresses. To compose the training data, we tap into our library of distinct SiCOH structures of different compositions that we have accumulated over the last two decades. It includes configurations of various polysiloxanes with standard side groups (H, CH_3, C_5H_6), hypothetical crystalline structures of SiCO with different compositions,[23] models of amorphous SiCO with and without "excess" carbon,[16, 21-22] and trajectories from *ab-initio* molecular dynamic (aiMD) simulations of Si-C-O-H polymers and SiCOH structures at elevated temperatures. Overall, the library covers a configurational space ranging from local minima to snapshots taken from dynamic simulations at 3000 K. We use the built-in active selection functionality of MLIP-2 to select critical configurations and avoid feeding the algorithm with repetition. Hence, we

For Peer Review

systematically improved the training set, focusing on low-temperature configurations first and then augmenting it with configurations at high temperatures. For example, we recently observed fundamental reaction mechanisms (including Kumada-like rearrangements) in aiMD simulations of siloxanes.[47] Significant parts of those trajectories are included in our training set for the MLIPs.

All configurations have been recalculated with identical parameters to obtain consistent energies, forces, and stresses for the machine-learning procedure. We used the Vienna ab initio Simulation Package (VASP)[48-50], with the projector augmented wave (PAW) method[51-52] and the Generalized Gradient Approximation as parametrized by Perdew, Becke, and Ernzerhof (PBE)[53-54] augmented by the universal correction method for dispersion corrections.[55] A cut-off of 500 eV is used to expand the wave function into plane wave basis sets. If structure optimizations are performed, forces are converged to 5 meV/Å for models smaller than 80 atoms and 0.1 eV/Å if larger. The reciprocal space is sampled to better than $0.04 \cdot 2\pi$/Å. We use the Γ-point only for models larger than 80 atoms.

We use passive and active learning strategies integrated within the MLIP-2 software. The passive strategy uses the provided DFT data only and obtains parameters suitable to describe the configurations as provided. For additional "on-the-fly" active learning, the MLIP-2 code interfaces with the LAMMPS [Large-scale Atomic/Molecular Massively Parallel Simulator][56] code to perform molecular dynamic (MD) simulations (NVT, time-step Δt=1 fs). The choice of temperature in LAMMPS was T=300 K for low-temperature and T=2500 K for high-temperature simulations. We implemented another independent LAMMPS-VASP loop as a "self-learning" strategy. [28] At low temperatures, without bond breaking, the loop must provide equivalent local configurations after simulations using the MLIP or by aiMD, while "divergence" identifies configurations to be added to the training set. After careful selection and further optimization of the procedure concerning efficiency and necessity, the final training set used in this study consists of 3,417 different structures comprising 503,885 atoms (and their forces). Note that this is, on average, 148 atoms per structure.

For Peer Review

Gauging the quality of the MLIPs is performed in the following way. The MTP formalism allows various flavors of complexity, resulting in different numbers of parameters in the final MLIP.[45] For instance, the cutoff radius, our final choice is 4.25 Å, impacts the complexity and speed of the MLIP. The main focus here addresses the "level variant" of the MTPs. Ultimately, we settled with a level–12 MTP, but we also developed and worked with level–20, –22, and –26. The level-12 MTP we showcase below contains more than 1100 parameters, the level-22 MTP comprises more than ten times as many. A practical gauge of comparison is visualized below in Figure 1. It compares the fidelity of force calculations – in the way of differences of force magnitude acting on an atom computed for the same configuration using the two different methods, f_{MTP}–f_{DFT} – for MTPs with level–12, –20, and –22 at low (800 K) and high (2500 K) temperatures. Our choice of the x–y axes facilitates an easy visual alignment of the 2D data to the 1D distribution (histogram) frequently shown.[57]

For Peer Review

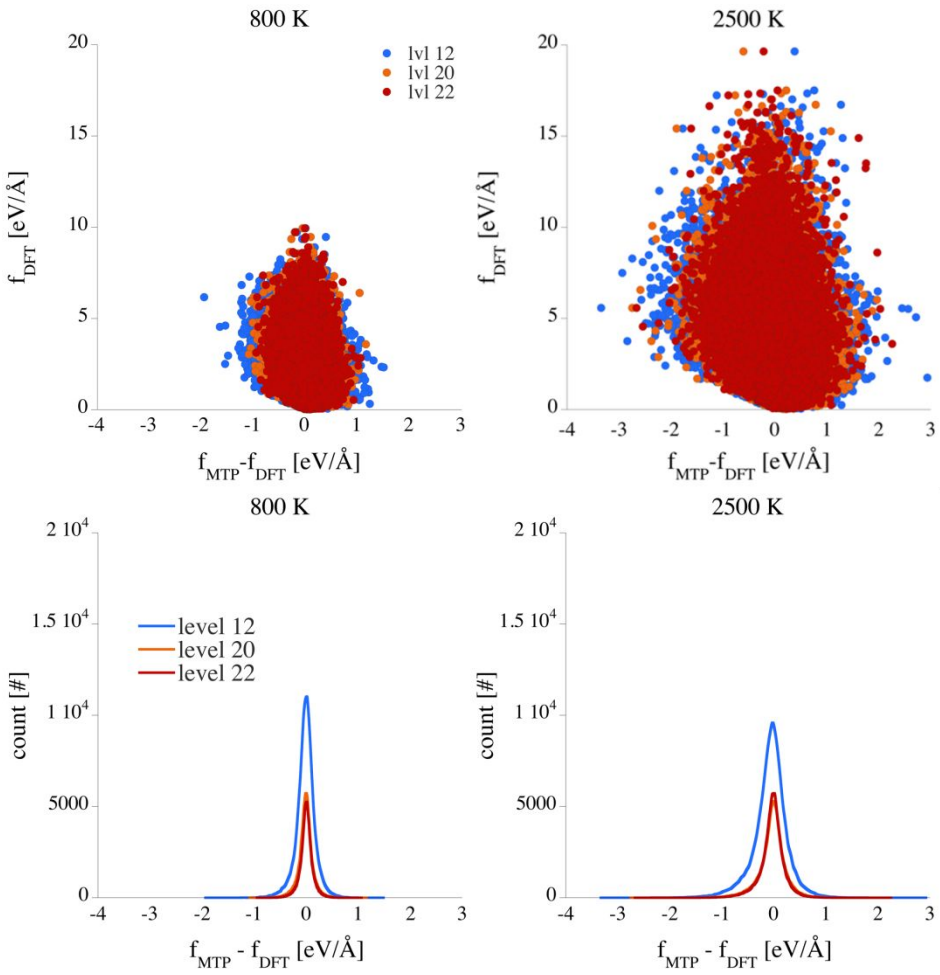

Figure 1: Visualizing DFT force magnitude f_{DFT} versus differences between MTP force magnitude and DFT force magnitude, f_{MTP}–f_{DFT}. The top row shows the data for temperatures of 800 K (left) and 2500 K (right) using individual dots for each data point. The bottom row displays the distribution of the force magnitude difference. The data is generated from the forces acting on each atom collecting several structures. Level–12, –20, and –22 are indicated in blue, orange, and red, respectively. Level–20 and –22 generate virtually identical distributions.

As expected, the fidelity of force calculations (e.g., decrease of the width) increases as the level of the MTP increases. This is seen by a smaller distribution width (bottom row) as the level increases. In addition, as the temperature increases, the overall uncertainty in force calculation increases. However, the largest differences f_{MTP}–f_{DFT} do not occur for the largest forces, which typically appear in reactions (e.g., bond breaking). With an eye on the computational effort – the simulation time for a level–20 MTP increases ~6-fold, that of a level–22 already ~10-fold over

that of level–12 – we decided to obtain results for this study using the level-12 MTP as our MLIP.

3 Results

This study's scope is developing a machine–learning interatomic potential (MLIP) for the simulation of pre-ceramic SiCOH polymers, their pyrolysis, and products. We split our results into two sections: modeling low-temperature dynamics through vibrational spectra and simulating polymer degradation and reactions in the high-temperature range. Throughout this section, we present results for the level–12 MTP only.

3.1 Simulations at low temperature

We first consider vibrational densities of states (vDOS) for models of polydimethyl– and polydiphenylsiloxane (3D rod-packing of PDMS and PDPhS), a model of a–SiO_2:C_f with embedded graphitic carbon (lacking hydrogen), and a large SiCO(:H) structure generated via simulated pyrolysis of PDPhS. For polymeric structures, we look for signatures originating from the Si-O backbone and from substituents (Si-C and C-H). For the structures with free carbon, we separate the carbon atoms into "graphitic carbon", which we define as C with 3-fold coordination to C, and other C (e.g. interfacial or "disordered"). The vDOS are computed through velocity autocorrelation functions obtained from dynamic simulations at 300 K using VASPKIT.[58] For both methods, MLIP and aiMD simulations, we used an NVT ensemble, a time-step of 0.25 fs, and simulated 20 ps (80,000 steps) to provide a direct comparison. However, in difference to the development and training of the MLIP, the aiMD simulations here apply softer pseudopotentials and a cutoff of 280 eV only. For the a–SiO_2:C_f model with 793 atoms, we performed only 10 ps (40,000 steps).

In Figure 2, we compare the results obtained using MLIP and aiMD simulations. We observe remarkable agreement of vibrational states, with the MLIP data closely resembling the DFT results. Significant vibrations – C–H stretching, Si–CH_3 states, O-dominated vibrations of the siloxane backbone, and signatures resembling D- and G-peaks in graphite – are well captured

For Peer Review

by MTP. To some extent, this could be expected because snapshots of some dynamic simulations were part of the training set. For polydimethylsiloxane, PDMS, we find characteristic C–H localized vibrations at ~3100 cm^{-1}, 1450 cm^{-1}, and 1140 cm^{-1}. In addition, we observe vibrations of the polymer backbone, Si–O vibrations with dominant contribution by O, at 1050 cm^{-1}. Vibrations located within the $Si–CH_3$ unit appear at 800 cm^{-1}. The split peak at ~ 3100 cm^{-1} observed in DFT is merged into a single distribution of vibrations in MTP for both H and C contributions. A merging of peaks occurs in other instances as well, at ~ 1000 and 350 cm^{-1}. In the case of polydiphenylsiloxane, PDPhS, we find C–H stretching vibrations at ~3100 cm^{-1}, and a set of states between 1280 and 1550 cm^{-1} localized within the phenyl group. The Si–O vibrations of the polymer backbone again appear at ~1050 cm^{-1}. Vibrations originating from the $Si–C_6H_5$ group are found at 760 cm^{-1}. The participation of Si in these states is much stronger in PDPhS compared to similar states observed at about the same wavenumber in PDMS due to the higher effective mass of the C6H5 group relative to the CH_3 group.

The $a–SiO_2:C_f$ model is particularly helpful in characterizing the vibrational signature of (potentially existing) interfacial Si–C bonds. Note that C atoms in this model are either surrounded by three other C ($C-C_3$, then called “graphitic”) or bond to one Si and two C, $C–SiC_2$. The vDOS obtained with the MLIP agrees well with the data obtained using aiMD simulations. Both spectra reveal a clear difference in the vibrational signatures of $C-C_3$ versus $C–SiC_2$. This is an essential difference as it refers to the onset and extent of carbon segregation in SiCO ceramics during pyrolysis and annealing.[59] Only $C-C_3$ shows notable contributions in the range 1350–1600 cm^{-1}. The vDOS obtained by aiMD reflects D– and G-peaks observed for many carbon-rich SiCO materials.[30] Interfacial C, with at least one bond to Si, does not provide significant contributions in this range but typically shows up at significantly lower wave numbers, 1100-1300 cm^{-1}. Assuming a localized perspective, this is due to a much weaker/softer C-Si bond at the interface than a C-C bond inside graphite. Vibrations of the SiO_2 host structure appear in the range typical for silica (1100 cm^{-1}). Overall, the agreement of vDOS between MLIP and aiMD

For Peer Review

(DFT) is consistent and compelling. There are a few differences, typically at very low frequencies, not at least due to limited simulation times and truncated Fourier transformations.

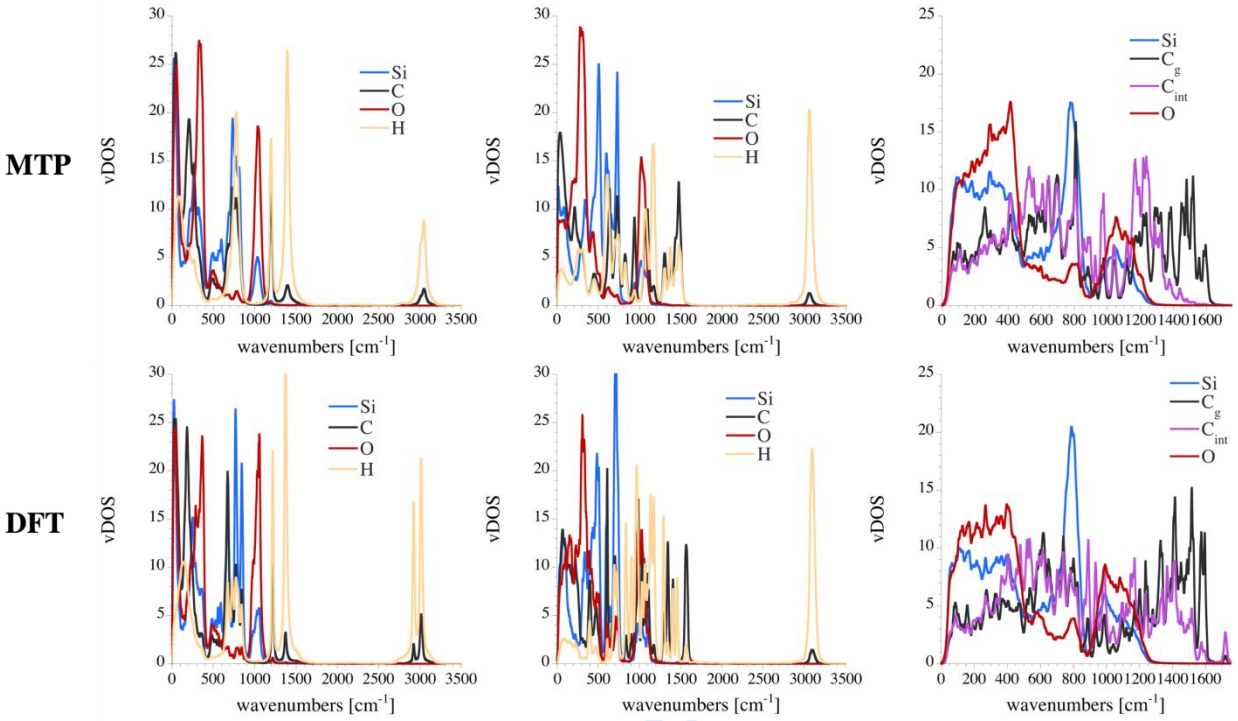

Figure 2: The upper row displays vDOS spectra generated using the MTP for each structure, PDMS, PDPhS, and the model of a–SiO_2:C_f. The lower row shows the corresponding vDOS spectra generated from aiMD simulations. We display partial projections corresponding to each atom type, Si, O, and H, as blue, red, and yellow lines, respectively. For C, we use purple and black lines. The data was generated using VASPKIT.[58]

Provided with some confidence in vibrational results obtained using the MLIP, we turn to the vDOS obtained for a model of pyrolyzed PDPhS. The process of pyrolysis simulations is described in the next section, albeit for a significantly larger model of PDPhS. The model analyzed here comprises 1,945 atoms and exhibits a sizeable two-dimensional C segregation embedded in a SiCO host matrix; see Figure 3 on the right. Individual graphene sheets are woven into each other, providing connectivity between the layers of the C-segregation. The limited size of the simulation cell (2.8 nm) might impact the particular segregation pattern.[29] The carbon layers also bond to the surrounding host via C–Si bonds. The vDOS presented in Figure 3 shows

C–H stretching vibrations at ~3100 cm^{-1}, as some H atoms are still present in this model. The most distinguished signal arises from C–C_3 environments and is found for wavenumbers between 1300 and 1600 cm^{-1} – the region that displays characteristic D– and G–peaks of graphitic segregations in SiCO.[30] A few states related to two-fold coordinated C atoms appear at ~1700 cm^{-1}, indicating that this model is still an "intermediate reaction product". Vibrational states with significant participation of C also appear at ~1200 cm^{-1}. These are due to interfacial C-Si bonds. O-centered states at ~1050 and a signature at ~800 cm^{-1} assigned to vibrational states with Si and C participation indicate the presence of the SiCO host structure.

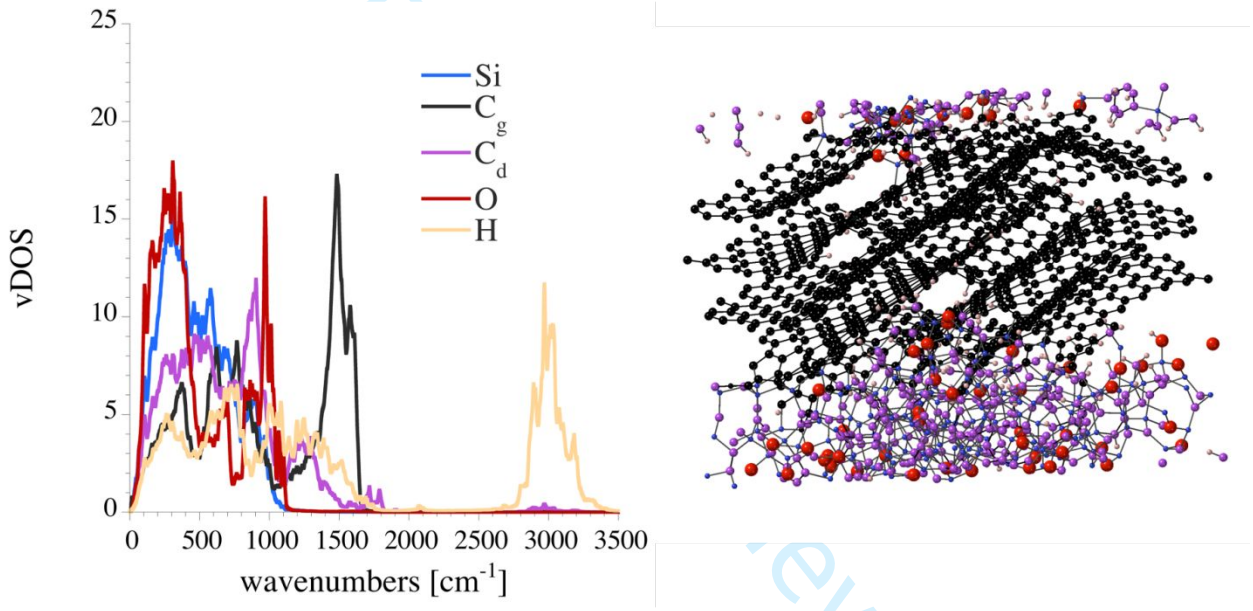

Figure 3: Model of pyrolyzed PDPhS displaying a segregation of "free" carbon. On the left, the vDOS is computed at 300K using classical MD simulation with the MLIP. Lines show partial contribution from Si, C, O, and H. Blue, red, and yellow lines represent Si, O, and H. C atoms with C-C_3 environment are represented black, others magenta. The right shows the structure after pyrolysis. Si, C, O, and H are shown in blue, black/magenta, red, and pink.

Overall, we observe a remarkable alignment of low-temperature vibrational spectra obtained by ab initio (DFT) MD simulations and by MD simulations using the MLIP. Vibrational properties are excellent observables and allow comparison to experimental data. The usefulness of the MLIP becomes apparent, as it computes the vibrational data within a fraction of time compared

to the far more expensive aiMD simulation. This way, it becomes possible to model a variety of configurations – in particular, different hypotheses of carbon segregations within SiCO materials[59] – and analyze their respective vibrational pattern. Identifying differences (e.g., the signature of "interfacial C-Si bonds or the onset of developing a "G-peak") will then help to understand the segregation process of "free" carbon. As mentioned before, this outcome of the MLIP generation could be expected because the machine learning process involves just the configurational sampling of localized bonding environments. We remark that framework vibrations with low wavenumbers are still challenging to model properly. These typically involve weaker interaction over larger distances, features not well addressed by our DFT calculations in limited-size models used to build the training set.

3.1 High-temperature simulations

Turning to high-temperature properties, we highlight results of high-temperature simulations of typical polysiloxanes that we performed using the MLIP. We start showing examples of the development of so-called "mixed tetrahedra", SiC_nO_{4-n}–environments that are typical for describing the state of the SiCO glass phase.[60] We built a polydimethylsiloxane (PDMS) model comprising infinite polymer strands in a 3-dimensional rod packing. The structure started with the composition $Si_{2304}C_{4608}O_{2304}H_{13824}$ (= 2304 · SiC_2OH_6) and a density of 1.0 g/cm^3. After briefly heating, we developed the model at 1400 K and 2000 kbar for 100 ns using a time step Δt=1 fs. During the simulation, the system evolves gaseous molecules, and the polymer undergoes a transformation (pyrolysis) into a ceramic-like state. We remove gaseous species SiH_4, $Si_2O(CH_3)_6$, $Si(CH_3)_3OH$, $Si_2CH_2(CH_3)_6$, $Si(CH_3)_4$, CO_2, CO, CH_4, C_2H_2, C_2H_4, C_2H_6, C_6H_6, CH_2O, O_2, H_2O, CH_3OH, and H_2) from the system every 100 ps using a probabilistic approach inspired by Graham's law. The probability p_{gas} to remove a gas molecule with mass m_{gas} is given by $p_{gas} = \sqrt{\frac{m_{H_2}}{m_{gas}}}$. After 100 ns, the composition of the system is $Si_{2290}C_{2352}O_{2284}H_{4780}$ or $Si_{1.0}C_{1.0}O_{1.0}H_{2.1}$. Thus, a lot of hydrogen is still present in the system. Figure 4 shows the progress of SiC_nO_{4-n}–environments during the simulation. The mixed SiC_nO_{4-n}–tetrahedra are labeled by letters following the standard convention of Q, T, D, M, and X for n=0, 1, 2, 3, 4, respectively.

For Peer Review

Note that the distribution of mixed tetrahedra in a random bond model follows random statistic, with $p(SiC_nO_{4-n}) = \frac{4!}{(4\text{-}n)!n!} p_{Si\text{-}O}{}^{4\text{-}n} p_{Si\text{-}C}{}^{n}$. The Si–O and Si–C bond probabilities are computed from the composition x·SiC + (1-x)·SiO_2 of the glass phase, $p_{Si\text{-}O}$=(1-x)/2 and $p_{Si\text{-}C}$=1-$p_{Si\text{-}O}$. The PDMS model starts with only D sites, but significant parts of these soon convert according to the redistribution reaction 2D → M + T. In addition, the pyrolysis reactions form new bonds and create new environments. After 100 ns simulation at 1400 K, we observe a distribution of $SiC_nO_{4\text{-}n}$–tetrahedra with 2.4 (6.2), 25.8 (24.9), 50.1 (37.5), 20.4 (25.1), 1.3 (6.3) %, for n=0,1,2,3,4, respectively, with the values for a perfect random network given in parentheses. With ongoing chemical reactions, the system steadily approaches the "ideal" random network distribution.

In another simulation, we perform the same analysis of the distribution of $SiC_nO_{4\text{-}n}$–tetrahedra during pyrolysis of polymethylhydrosiloxane (PMHS). The simulation parameters were similar to those for PDMS, but we heated the system to 2500 K instead this time. In this simulation, we prevented the removal of CH_4 and H_2O. The evolution of the distribution of $SiC_nO_{4\text{-}n}$–tetrahedra in this system is shown in Figure 4 on the right side. The data fluctuates significantly more in this simulation due to the higher temperatures. The average values computed for snapshots taken between 150–200 ns for the distribution of $SiC_nO_{4\text{-}n}$–tetrahedra are 6.3 (5.6), 26.0 (23.7), 38.6 (37.4), 23.8 (26.3), and 5.3 (6.9) %, for n=0,1,2,3,4, respectively. As before, the values in parentheses are those for a perfect random network. Note that the system is still evolving, and the amounts of SiC_4– and SiO_4–tetrahedra are continuously increasing.

For Peer Review

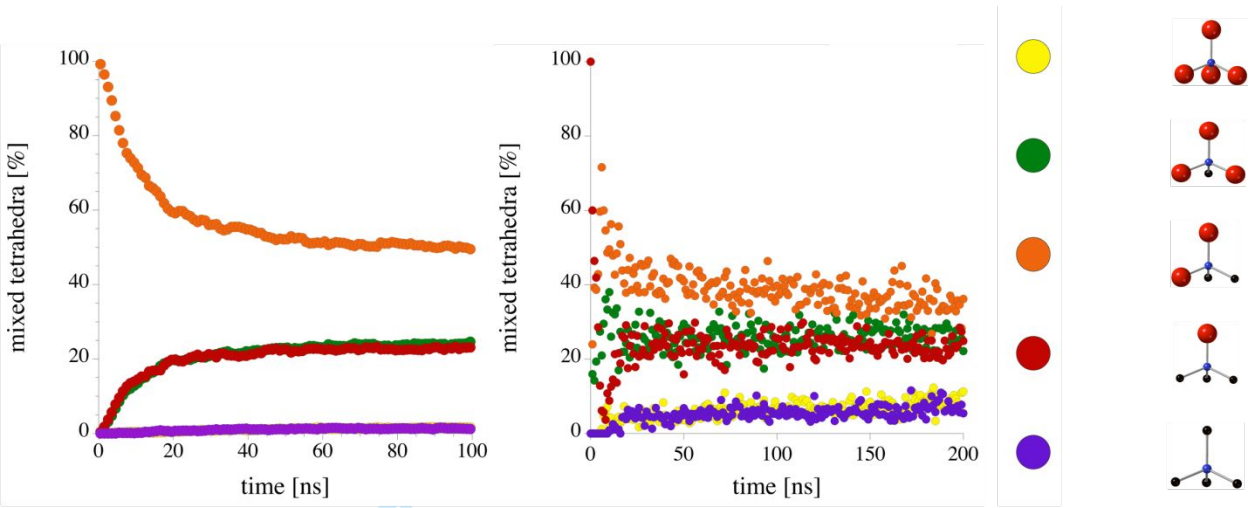

Figure 4: Distributions of SiC_nO_{4-n}–tetrahedra observed during pyrolysis simulation of PDMS and PMHS shown on the left and the right, respectively. The color codes and local configurations of "mixed" SiC_nO_{4-n}–tetrahedra tetrahedra are displayed to the right. Si, C, and O are shown in blue, black, and red.

Moving further to high-temperature pyrolysis simulations, we address a large SiCO system with significant "excess carbon". We built a model of polydiphenylsiloxane (PDPhS), comprising a 3D rod packing of 8-mers, with composition $Si_{41472}C_{414720}O_{41472}H_{497664}$ (= 41472 · $[SiO(C_5H_6)_2]$). Hence, the initial model includes about 1 million atoms. After increasing the temperature, we simulated 2500 K under constant pressure (8000 kbar) for 10 nanoseconds. We removed gaseous species every 10 ps using the "Graham-inspired" method described above. After 10 ns simulation time, the system has the composition $Si_{41472}C_{367124}O_{9114}H_{57248}$ or $SiC_{8.9}O_{0.2}H_{1.4}$. The size of the corresponding simulation box is 17.9 nm. The model after 10 ns comprises about 292,864 C atoms with three or two bonds to other C. We selected those as the "free" carbon phase and show them in Figure 5.

For Peer Review

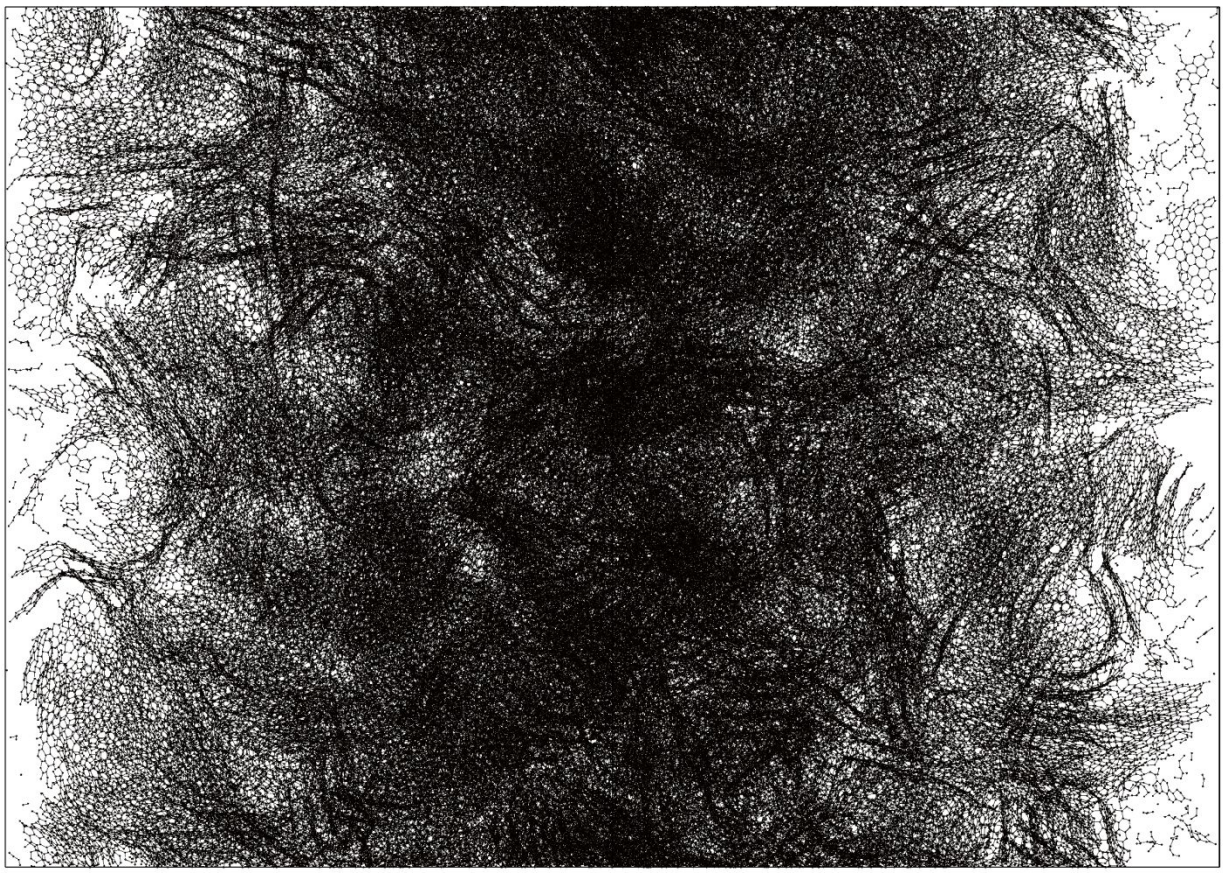

Figure 5: The "Free" carbon phase is observed in a pyrolysis model of PDPhS after 10 ns at 2500 K. Only those C atoms of the structure at least two-fold coordinated to other C atoms are shown (292,864 C). Other C atoms and all Si, O, and H atoms are omitted. The cubic simulation box (a ≈ 17.9 nm) is rotated by 45° to facilitate the view along the "thin" edges, where the background is small enough to decipher individual sheets and stacked layers.

The model allows us to identify individual graphene layers that formed during pyrolysis. Most layers display curvature; in some cases, layers form small tubes. Stacked layers also occur, with a typical distance between layers of 3.2–3.9 nm. Note that there is still a small amount of SiCO and some H dispersed throughout the structure, which is not shown in the structure.

Our third example highlights detailed local chemical reactions found on trajectories generated during MD simulations using the MLIP. We isolated a process in which methane gas is formed, leaving behind a bridging Si-CH_2-Si, as shown in Figure 6. We observed this reaction in a classical MD NVT simulation of a model of PDMS at 1400K. The process itself begins with the

formation of 3-coordinated Si. This reactive Si then bridges to its second-nearest neighbor Si via a methyl group, forming a short-lived Si-CH_3-Si intermediate. The extra H migrates further and bonds with a methyl group, forming CH_4. The 3-coordinated Si left behind eventually finds a fourth partner in an adjacent Si's reactive CH_2. The initial steps, including the CH_4 abstraction, of this and similar processes happen within ~100 fs. In contrast, the final step of saturating the Si often takes one or two orders of magnitude longer to complete.

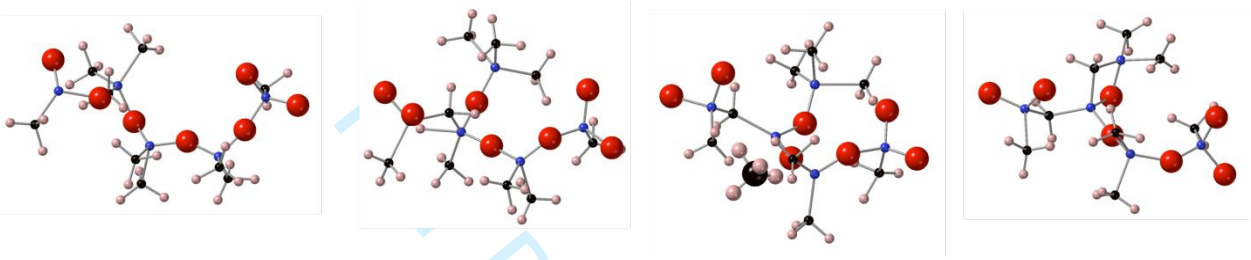

Figure 6: Still images of the trajectory of a process generating methane, CH_4. Atoms irrelevant to the reaction are omitted in this display. Initially, a CH_3 migrates from one Si to another, creating a 3-coordinated Si as an intermediate. The Si quickly finds an adjacent CH_3, forming a Si-CH_2-Si bridge and a very long Si…H interaction. This H joins a methyl group on the Si, forming CH_4 (displayed by a fat C atom). The 3-coordinated Si left behind eventually forms another Si-CH_2-Si linkage. Si, C, O, and H are shown in blue, black, red, and pink, respectively.

For the last demonstration of detailed high-temperature reactions, we turn to a specific mode of reorganization that is essential during the pyrolysis of polysiloxanes: the integration of carbon atoms originating from organic side groups into the siloxane polymer backbone. The process is similar to the Yajima process, which converts a polysilane into a polycarbosilane by migrating one of the methyl substituents into the polymer chain.[61] This migration is known as Kumada rearrangement and was first characterized for simple silane molecules such as hexamethyldisilane.[47] In polysiloxanes, the corresponding rearrangement inserts C from an aliphatic ligand on Si, typically a CH_3 group, into the Si–O–Si polymer backbone. We refer to this process as "Kumada-like" due to its resemblance with the original Kumada rearrangement. We observed this rearrangement multiple times during extensive aiMD simulations of PDMS and PMHS at elevated temperatures and could extract isolated processes without overlapping

secondary reactions. As mentioned earlier, we included selected configurations from the trajectory in our training set of the MLIP. Performing dynamic simulations of PDMS at elevated temperatures using the MLIP, we then observe several instances of a migration of a methylene group into the siloxane backbone. One such process is shown by individual snapshots of the trajectory in Figure 6. The process occurs over the course of several 100fs (here at 2500 K). A 5-coordinated Si and a 5-coordinated C are observed as short-living intermediates during the transition.

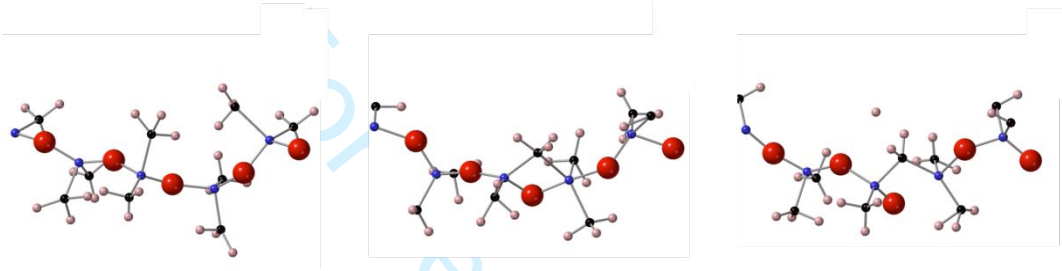

Figure 7: Snapshots (still images) along the trajectory of a Kumada-like rearrangement in polydimethylsiloxane. Atoms irrelevant to the reaction are omitted in this display. The methyl group at the center of each individual still image migrates from one Si to form a five-coordinated intermediate with the adjacent Si. Note that the second Si transformed its local environment from SiC_2O_2 to SiC_3O, hence D -> T, while the other Si retained its environment. Si, C, O, and H are shown in blue, black, red, and pink, respectively.

4 Discussion

The results demonstrate that the machine–learning interatomic potentials (MLIPs) that we developed are capable of dynamic simulations of Si-C-O-H compounds. Such simulations target structure and low-temperature vibrational properties but also include detailed chemical reactions occurring at high temperatures. The MLIPs were generated using MTPs and fitted to energies, forces, and stresses of DFT data. Additional active-learning techniques further augmented the training set “on the fly” and improved the MLIPs. Due to the diversity of the training data, the potential has a large applicability range. It can describe the formation of SiCO compounds and their properties in a large temperature and pressure range.

We demonstrate that the MLIP successfully reproduces vibrational properties of SiCOH obtained from aiMD simulations. This motivates us to appraise the quality of the MLIP simulations as having a "DFT-like" quality. With fidelity in the method established, it is possible to investigate significantly larger models that comprise structural features that cannot be captured in small models and computed using DFT. For example, detailed investigations are required of the genesis of carbon segregations in SiCO ceramics and of the interface between segregated carbon and the surrounding SiCO host matrix.[59] Such studies shall work out observables that can be measured in experiments, and a comparison of computational and experimental data will discriminate between different models that have been proposed.

The MLIP also simulates the conversion of polymers into SiCO ceramics at high temperatures. The distribution of tetrahedra aligns well with the expectations of the SiCO glass phase that have been established in many experimental studies. We also demonstrate a simulation starting with 1,000,000 atoms and developing the system for 10 ns. This large-scale simulation features a model in a simulation box with box length a ≈ 17.9 nm and volume of V ≈ 6400 nm^3. While this is still a microscopic model, it will allow studying the segregation and formation of different phases in SiCO with high accuracy at unprecedented length and time scales.

Compared to aiMD simulations, the MLIPs are significantly faster and, in addition, allow much larger length scales to be addressed. Compared to reactive simulations using ReaxFF with the parameters we developed earlier,[28] we estimate that the MLIP is about 40 times faster per time step of the simulation. Since ReaxFF requires careful time step adjustment for both the integration of the equations of motion and the charge equilibration, we find the overall speed-up even higher.

The provided MLIPs are not perfect and will need to be developed further. There are fundamental challenges to MLIPs, for example the mobility of charges or spins, that impact all reactive systems.[39] A noticeable imperfection of the MLIPs presented here is a low reactivity of CH_4 and H_2O molecules once these are generated. This behavior becomes visible only in more

For Peer Review

extended simulations and if gaseous molecules are removed. Eventually, the molecules will react even with the MLIP. A comparison to aiMD simulation that we performed for up to 1 ns, however, indicates too slow kinetics of reactions of these molecules. Adding selected configurations of reaction trajectories obtained from additional aiMD simulation will help to remedy this issue in the future. Another imperfection we observed is a high abundance in C-Si_3– environments in the SiCO glass phase after the final optimization of a model. Subsequent spin-polarized DFT optimization of such geometries yields a high population of unpaired spins, indicating high magnetization. We note that all the observed imperfections became visible only after extended MD simulations, which is why current active-learning strategies cannot address such situations "on the fly". Despite these imperfections, the MLIPs here deliver simulations of polysiloxanes and SiCOH ceramics with unprecedented quality and form a tool to advance understanding of the chemical and structural development in such complex systems.

4 Summary

In this contribution, we show the development of Machine–Learning Interatomic Potentials (MLIPs) for simulations of polysiloxanes and SiCO ceramics based on Moment-Tensor-Potentials (MTPs). Taking advantage of our extensive library of SiCOH configurations, we trained the MLIPs to polymer structures, crystalline and amorphous SiCOH structures, and included trajectories of ab-initio molecular dynamic (aiMD) simulations of SiCOH structures at elevated temperatures. Beyond passive training to energies, forces, and stresses, we applied active-learning strategies and implemented further hybrid learning to improve the MLIPs. The results demonstrate that the MLPs simulate low-temperature properties of polysiloxanes and SiCOH ceramics with "DFT-like" quality. Beyond properties close to a local minimum configuration, we show examples of simulations of the polymer-to-ceramic transformation. Individual chemical reactions become visible and can be studied in detail, and million-atom simulations extending over several nanoseconds are feasible. The structural development of mixed tetrahedra in SiCO ceramics and the precipitation of nanometer-sized graphitic

For Peer Review

segregations in C-rich SiCO systems align with experimental observations, demonstrating a high fidelity of the MLIPs. We have also identified some imperfections of the MLIPs that can be remedied in future systematic improvement. Overall, the MLIPs deliver "DFT-like" quality in multi-million atom simulations of SiCOH for modeling nanoscale structures and pyrolysis simulations extending for several nanoseconds.

Acknowledgment

This work used Expanse at San Diego Supercomputer Center (SDSC) and Stampede2 and Lonestar6 at Texas Advanced Computing Center (TACC) through allocation DMR190103 from the Advanced Cyberinfrastructure Coordination Ecosystem: Services & Support (ACCESS) program, which is supported by National Science Foundation grants #2138259, #2138286, #2138307, #2137603, and #2138296. Significant contributions of earlier results were obtained at the same systems through allocation DMR190103 from the Extreme Science and Engineering Discovery Environment (XSEDE), which was supported by National Science Foundation grant number #1548562. Additional computational work was made possible by the High-Performance Computing facilities at UTA. This work was partially supported by the National Science Foundation (NSF) through award #1743701.

For Peer Review

References

1. Nguyen, M. D.; Bang, J. W.; Bin, A. S.; Kim, S.-R.; Kim, Y.; Hwang, K. H.; Pham, V.-H.; Kwon, W.-T., Novel Polymer-Derived Ceramic Environmental Barrier Coating System for Carbon Steel in Oxidizing Environments. *Journal of the European Ceramic Society* **2017**, *37*, 2001-2010.
2. Stabler, C.; Ionescu, E.; Graczyk-Zajac, M.; Gonzalo-Juan, I.; Riedel, R., Silicon Oxycarbide Glasses and Glass-Ceramics: "All-Rounder" Materials for Advanced Structural and Functional Applications. *Journal of the American Ceramic Society* **2018**, *101*, 4817-4856.
3. Liu, C.; Pan, R.; Hong, C.; Zhang, X.; Han, W.; Han, J.; Du, S., Effects of Zr on the Precursor Architecture and High-Temperature Nanostructure Evolution of Sioc Polymer-Derived Ceramics. *Journal of the European Ceramic Society* **2016**, *36*, 395-402.
4. Fukui, H.; Ohsuka, H.; Hino, T.; Kanamura, K., A Si−O−C Composite Anode: High Capability and Proposed Mechanism of Lithium Storage Associated with Microstructural Characteristics. *ACS Applied Materials & Interfaces* **2010**, *2*, 998-1008.
5. Lee, J.; Jang, W.; Kim, H.; Shin, S.; Kweon, Y.; Lee, K.; Jeon, H., Characteristics of Low-K Sioc Films Deposited Via Atomic Layer Deposition. *Thin Solid Films* **2018**, *645*, 334-339.
6. Vakifahmetoglu, C.; Zeydanli, D.; Innocentini, M. D. d. M.; Ribeiro, F. d. S.; Lasso, P. R. O.; Soraru, G. D., Gradient-Hierarchic-Aligned Porosity Sioc Ceramics. *Scientific Reports* **2017**, *7*, 41049.
7. Merida, J.; Colomer, M. T.; Rubio, F.; Mazo, M. A., Highly Porous Carbon Materials Derived from Silicon Oxycarbides and Effect of the Pyrolysis Temperature on Their Electrochemical Response. *Int J Mol Sci* **2023**, *24*.
8. Tamayo, A.; Mazo, M. A.; Ruiz-Caro, R.; Martín-Illana, A.; Bedoya, L. M.; Veiga-Ochoa, M. D.; Rubio, J., Mesoporous Silicon Oxycarbide Materials for Controlled Drug Delivery Systems. *Chemical Engineering Journal* **2015**, *280*, 165-174.
9. Soraru, G.; Pederiva, L.; Latournerie, J.; Raj, R., Pyrolysis Kinetics for the Conversion of a Polymer into an Amorphous Silicon Oxycarbide Ceramic. *Journal of the American Ceramic Society* **2004**, *85*, 2181-2187.
10. Jana, P.; Santoliquido, O.; Ortona, A.; Colombo, P.; Sorarù, G. D., Polymer-Derived Sicn Cellular Structures from Replica of 3d Printed Lattices. *JOURNAL OF THE AMERICAN CERAMIC SOCIETY* **2018**, *101*, 2732-2738.
11. Kemp, J. W.; Reed, J. L.; Compton, B. G., Size Effects in 3d-Printed Polymer-Derived, Zirconium Diboride-Reinforced Ceramic Composites. *JOURNAL OF THE AMERICAN CERAMIC SOCIETY* **2024**, *107*, 1557-1570.
12. Monte, F. A. D.; Awad, K. R.; Ahuja, N.; Kim, H. K. W.; Aswath, P.; Brotto, M.; Varanasi, V. G., Amorphous Silicon Oxynitrophosphide-Coated Implants Boost Angiogenic Activity of Endothelial Cells. *Tissue Eng Part A* **2020**, *26*, 15-27.

For Peer Review

13. Bai, W. R.; Widgeon, S.; Sen, S., Structure and Topological Characteristics of Amorphous Silicon Oxycarbide Networks: Results from Reverse Monte Carlo Simulations. *JOURNAL OF NON-CRYSTALLINE SOLIDS* **2014**, *386*, 29-33.
14. Widgeon, S. J.; Sen, S.; Mera, G.; Ionescu, E.; Riedel, R.; Navrotsky, A., 29si and 13c Solid-State Nmr Spectroscopic Study of Nanometer-Scale Structure and Mass Fractal Characteristics of Amorphous Polymer Derived Silicon Oxycarbide Ceramics. *Chemistry of Materials* **2010**, *22*, 6221-6228.
15. Saha, A.; Raj, R.; Williamson, D. L., A Model for the Nanodomains in Polymer-Derived Sico. *Journal of the American Ceramic Society* **2006**, *89*, 2188-2195.
16. Kroll, P., Modeling the 'Free Carbon' Phase in Amorphous Silicon Oxycarbide. *JOURNAL OF NON-CRYSTALLINE SOLIDS* **2005**, *351*, 1121-1126.
17. Kleebe, H.-J.; Turquat, C.; Sorarù, G. D., Phase Separation in an Sico Glass Studied by Transmission Electron Microscopy and Electron Energy-Loss Spectroscopy. *Journal of the American Ceramic Society* **2001**, *84*, 1073-1080.
18. Mazo, M. A.; Soriano, D.; Rubio, J., Mechanical Response of Silicon Oxycarbide Materials Processed by Spark Plasma Sintering. *Ceramics International* **2023**, *49*, 12866-12875.
19. Colombo, P.; Mera, G.; Riedel, R.; Sorarù, G. D., Polymer-Derived Ceramics: 40 Years of Research and Innovation in Advanced Ceramics. *Journal of the American Ceramic Society* **2010**, *93*, 1805-1837.
20. Riedel, R.; Mera, G.; Hauser, R.; Klonczynski, A., Silicon-Based Polymer-Derived Ceramics: Synthesis Properties and Applications-a Review Dedicated to Prof. Dr. Fritz Aldinger on the Occasion of His 65th Birthday. *Journal of the Ceramic Society of Japan (日本セラミックス協会学術論文誌)* **2006**, *114*, 425-444.
21. Kroll, P., Modelling and Simulation of Amorphous Silicon Oxycarbide. *JOURNAL OF MATERIALS CHEMISTRY* **2003**, *13*, 1657-1668.
22. Kroll, P., Searching Insight into the Atomistic Structure of Sico Ceramics. *JOURNAL OF MATERIALS CHEMISTRY* **2010**, *20*, 10528-10534.
23. Bodiford, N. Crystalline SiCO: Implication on Structure and Thermochemistry of Ternary Silicon Oxycarbide Ceramics. Thesis; The University of Texas at Arlington; **2014**.
24. Nimmo, J. P.; Kroll, P., First-Principles Calculations and Analysis of Si-29 Nuclear Magnetic Resonance Chemical Shifts in Silicon Oxycarbide Ceramics. *JOURNAL OF PHYSICAL CHEMISTRY C* **2014**, *118*, 29952-29961.
25. Leimeroth, N.; Rohrer, J.; Albe, K., Structure-Property Relations of Silicon Oxycarbides Studied Using a Machine Learning Interatomic Potential. *Journal of the American Ceramic Society* **2024**. DOI10.1111/jace.19932.
26. Gao, H. F.; Wang, H. J.; Zhao, Z. H.; Niu, M.; Su, L.; Wei, Y., Reactive Dynamics Simulation Study on the Pyrolysis of Polymer Precursors to Generate Amorphous Silicon Oxycarbide Structures. *JOURNAL OF PHYSICAL CHEMISTRY C* **2018**, *122*, 5767-5773.
27. Ding, H. P.; Demkowicz, M. J., Hydrogen Reverses the Clustering Tendency of Carbon in Amorphous Silicon Oxycarbide. *SCIENTIFIC REPORTS* **2015**, *5*.

For Peer Review

28. Ponomarev, I.; van Duin, A. C. T.; Kroll, P., Reactive Force Field for Simulations of the Pyrolysis of Polysiloxanes into Silicon Oxycarbide Ceramics. *The Journal of Physical Chemistry C* **2019**, *123*, 16804-16812.
29. Haseen, S.; Kroll, P., Analyzing the Effect of Composition, Density, and the Morphology of the "Free" Carbon Phase on Elastic Moduli in Silicon Oxycarbide Ceramics. *Journal of the European Ceramic Society* **2023**, *43*, 1432-1441.
30. Mera, G.; Kroll, P.; Ponomarev, I.; Chen, J.; Morita, K.; Liesegang, M.; Ionescu, E.; Navrotsky, A., Metal-Catalyst-Free Access to Multiwalled Carbon Nanotubes/Silica Nanocomposites (Mwcnt/Sio2) from a Single-Source Precursor. *Dalton Transactions* **2019**, *48*, 11018-11033.
31. Bartók, A. P.; Payne, M. C.; Kondor, R.; Csányi, G., Gaussian Approximation Potentials: The Accuracy of Quantum Mechanics, without the Electrons. *Physical Review Letters* **2010**, *104*, 136403.
32. Bartók, A. P.; Kondor, R.; Csányi, G., On Representing Chemical Environments. *Physical Review B* **2013**, *87*, 184115.
33. Behler, J.; Parrinello, M., Generalized Neural-Network Representation of High-Dimensional Potential-Energy Surfaces. *Physical Review Letters* **2007**, *98*, 146401.
34. Drautz, R., Atomic Cluster Expansion for Accurate and Transferable Interatomic Potentials. *Physical Review B* **2019**, *99*, 014104.
35. Dusson, G.; Bachmayr, M.; Csányi, G.; Drautz, R.; Etter, S.; van der Oord, C.; Ortner, C., Atomic Cluster Expansion: Completeness, Efficiency and Stability. *Journal of Computational Physics* **2022**, *454*, 110946.
36. Thompson, A. P.; Swiler, L. P.; Trott, C. R.; Foiles, S. M.; Tucker, G. J., Spectral Neighbor Analysis Method for Automated Generation of Quantum-Accurate Interatomic Potentials. *Journal of Computational Physics* **2015**, *285*, 316-330.
37. Schütt, K. T.; Sauceda, H. E.; Kindermans, P. J.; Tkatchenko, A.; Müller, K. R., Schnet – a Deep Learning Architecture for Molecules and Materials. *The Journal of Chemical Physics* **2018**, *148*, 241722.
38. Batzner, S.; Musaelian, A.; Sun, L.; Geiger, M.; Mailoa, J. P.; Kornbluth, M.; Molinari, N.; Smidt, T. E.; Kozinsky, B., E(3)-Equivariant Graph Neural Networks for Data-Efficient and Accurate Interatomic Potentials. *Nature Communications* **2022**, *13*, 2453.
39. Behler, J.; Csányi, G., Machine Learning Potentials for Extended Systems: A Perspective. *The European Physical Journal B* **2021**, *94*, 142.
40. Shapeev, A. V., Moment Tensor Potentials: A Class of Systematically Improvable Interatomic Potentials. *Multiscale Modeling & Simulation* **2016**, *14*, 1153-1173.
41. Novikov, I. S.; Shapeev, A. V., Improving Accuracy of Interatomic Potentials: More Physics or More Data? A Case Study of Silica. *Materials Today Communications* **2019**, *18*, 74-80.
42. Novoselov, II; Yanilkin, A. V.; Shapeev, A. V.; Podryabinkin, E. V., Moment Tensor Potentials as a Promising Tool to Study Diffusion Processes. *COMPUTATIONAL MATERIALS SCIENCE* **2019**, *164*, 46-56.

For Peer Review

43. Zongo, K.; Sun, H.; Ouellet-Plamondon, C. M.; B'eland, L. K. In *A Unified Moment Tensor Potential for Silicon, Oxygen, and Silica*, 2023.
44. Podryabinkin, E. V.; Kvashnin, A. G.; Asgarpour, M.; Maslenikov, I. I.; Ovsyannikov, D. A.; Sorokin, P. B.; Popov, M. Y.; Shapeev, A. V., Nanohardness from First Principles with Active Learning on Atomic Environments. *Journal of Chemical Theory and Computation* **2022**, *18*, 1109-1121.
45. Novikov, I. S.; Gubaev, K.; Podryabinkin, E. V.; Shapeev, A. V., The Mlip Package: Moment Tensor Potentials with Mpi and Active Learning. *Machine Learning: Science and Technology* **2021**, *2*, 025002.
46. Podryabinkin, E.; Garifullin, K.; Shapeev, A.; Novikov, I., Mlip-3: Active Learning on Atomic Environments with Moment Tensor Potentials. *The Journal of Chemical Physics* **2023**, *159*, 084112.
47. Shiina, K.; Kumada, M., Notes - Thermal Rearrangement of Hexamethyldisilane to Trimethyl(Dimethylsilylmethyl)Silane. *The Journal of Organic Chemistry* **1958**, *23*, 139-139.
48. Kresse, G.; Hafner, J., Ab Initio Molecular Dynamics for Liquid Metals. *Physical Review B* **1993**, *47*, 558-561.
49. Kresse, G.; Furthmüller, J., Efficient Iterative Schemes for Ab Initio Total-Energy Calculations Using a Plane-Wave Basis Set. *Physical Review B* **1996**, *54*, 11169-11186.
50. Kresse, G.; Furthmüller, J., Efficiency of Ab-Initio Total Energy Calculations for Metals and Semiconductors Using a Plane-Wave Basis Set. *Computational Materials Science* **1996**, *6*, 15-50.
51. Blöchl, P. E., Projector Augmented-Wave Method. *Physical Review B* **1994**, *50*, 17953-17979.
52. Kresse, G.; Joubert, D., From Ultrasoft Pseudopotentials to the Projector Augmented-Wave Method. *Physical Review B* **1999**, *59*, 1758-1775.
53. Perdew, J. P.; Burke, K.; Ernzerhof, M., Generalized Gradient Approximation Made Simple. *Physical Review Letters* **1996**, *77*, 3865-3868.
54. Perdew, J. P.; Burke, K.; Ernzerhof, M., Generalized Gradient Approximation Made Simple [Phys. Rev. Lett. 77, 3865 (1996)]. *Physical Review Letters* **1997**, *78*, 1396-1396.
55. Kim, H.; Choi, J.-M.; Goddard, W. A., III, Universal Correction of Density Functional Theory to Include London Dispersion (up to Lr, Element 103). *The Journal of Physical Chemistry Letters* **2012**, *3*, 360-363.
56. Thompson, A. P., et al., Lammps - a Flexible Simulation Tool for Particle-Based Materials Modeling at the Atomic, Meso, and Continuum Scales. *Computer Physics Communications* **2022**, *271*, 108171.
57. Morrow, J. D.; Gardner, J. L. A.; Deringer, V. L., How to Validate Machine-Learned Interatomic Potentials. *The Journal of Chemical Physics* **2023**, *158*, 121501.
58. Wang, V.; Xu, N.; Liu, J.-C.; Tang, G.; Geng, W.-T., Vaspkit: A User-Friendly Interface Facilitating High-Throughput Computing and Analysis Using Vasp Code. *Computer Physics Communications* **2021**, *267*, 108033.

For Peer Review

59. Wen, Q.; Yu, Z.; Riedel, R., The Fate and Role of in Situ Formed Carbon in Polymer-Derived Ceramics. *Progress in Materials Science* **2020**, *109*, 100623.
60. Zhang, H.; Pantano, C. G., Synthesis and Characterization of Silicon Oxycarbide Glasses. *JOURNAL OF THE AMERICAN CERAMIC SOCIETY* **1990**, *73*, 958-963.
61. Murase, H.; Kawasaki, S.; Kitaoka, T.; Furukawa, J.; Ueda, H.; Nishimura, H.; Yamada, K., Effects of Polysilane-Coating on Interface of Electrofusion Joints for Maintaining Strength. *Materials Sciences and Applications* **2015**, *06*, 322-331.

For Peer Review

Dear Editor:

We are pleased with the reviewer's favorable view of the manuscript we prepared. The reviewer only suggested minor revisions, and we gladly considered their suggestions.

Here is our reply to the comments together with an indication of changes we did (as suggested, we use “track changes” in the manuscript; we also provide one version “final_revised”). We have prepared a revised manuscript, which we submit along with this letter.
What follows is a detailed response to the reports, with comments/queries of the reviewer in *italics*.

Comments from Reviewer #1:

Conclusion

The manuscript by Falgoust and Kroll is a significant contribution to the field of materials science, particularly in the computational modeling and simulation of ceramic materials. The successful application of MLIPs to this complex domain not only underscores the potential of machine learning to enhance traditional computational methods but also opens up new avenues for the development of advanced materials. The detailed presentation and robust validation of the MLIPs make this work a valuable reference for both researchers and practitioners in the field.

Overview

This manuscript presents a detailed and technically robust exploration of Machine-Learning Interatomic Potentials (MLIPs) used for the simulation of Si-C-O-H compounds, specifically focusing on polysiloxanes and their pyrolysis into SiCO ceramics. The research is comprehensive, employing a sophisticated blend of computational methods to train and validate the proposed MLIPs, anchored on a framework of Moment-Tensor-Potentials (MTPs).

Thanks to the reviwer.

Strengths

1. Technical Rigor: The manuscript offers a deep dive into the generation and application of MLIPs, demonstrating high fidelity in simulating complex chemical reactions and transformations relevant to ceramic materials engineering. The authors' use of an extensive training library incorporating DFT-calculated properties ensures the MLIPs' robustness.

2. Innovative Approach: The approach to integrating machine learning with traditional computational chemistry methods is noteworthy. This innovation not only enhances simulation speeds significantly compared to DFT methods but also maintains high accuracy, which is convincingly demonstrated through various comparative analyses presented in the manuscript.

3. Impact on the Field: The development of MLIPs for this class of materials could significantly advance the design and manufacturing of ceramic-based composites, with potential applications in industries where high-

performance materials are crucial. The authors effectively outline how their work can aid in understanding and improving the properties of SiCO ceramics.

Weaknesses

1. Complexity of Content: While the technical depth is a strength, it also makes the manuscript potentially inaccessible to readers not deeply versed in computational materials science. The authors could improve readability by simplifying explanations and perhaps including a more detailed glossary of terms and methodologies for non-specialist readers.

2. Limited Experimental Validation: The validation of the MLIPs relies heavily on comparison with other computational methods rather than experimental results. Including experimental validation could greatly enhance the credibility and acceptability of the models, particularly for practical applications.

Recommendations

1. Enhanced Clarity and Accessibility: The authors should consider revising the manuscript to make it more accessible to a broader audience by simplifying the more complex discussions and providing additional explanatory notes or supplementary material that outlines the basic concepts and methods used.

Sadly, the reviewer has not provided examples for “simplifying” the content, nor has the reviewer indicated " complex " sections that deserve simplification.
We believe that any reader looking for the meritorious outcome – the essence of the work – will (after reading the abstract) first study the result section. This part of our contribution, however, is rather “condensed” already and focuses on the bare necessities while providing appropriate references that connect to experimental outcomes (where possible).
It is, thus, only our guess that the comments refer primarily to technical details of the method section. However, how did we convince the reviewer of the “*Technical rigor*” of our work, if not by providing proper descriptions – rather than by using a “black-box approach”?
Nevertheless, we focused on the method section: we shortened it by several sentences, and we rewrote a few passages to enhance the reading experience in the technical section. These are indicated via “track changes” in the revised manuscript.

2. Experimental Validation: If possible, incorporating experimental data to corroborate the computational predictions could provide a stronger foundation for the MLIPs' applicability in real-world scenarios.

We have already provided several connections to experimental results. Common experimental observables are:
• vibrational spectroscopy — Figure 3: the appearance of a G-peak as a signature of segregated carbon. We are referencing the review article by Wen & Riedel and the experimental work by Mera. (note that so far there is no detailed study on “interfaces” between graphite and SiCO)
• distribution of mixed SiC_nO_{4-n}–tetrahedra — Figure 4: we are referring to the classical paper of Zhang and Pantano with ^{29}Si-NMR results.
• visible C-segregations — Figure 5: the foundational work of Kleebe (TEM of C segregations in the nm-range) is already included.

• incorporation of C into the Si–O backbone of the polymer — Figure 7.
Therefore, we are confident that these connections to experimental data support the validity of the MLIP provided.
We have avoided a repetition of the computation of elastic properties (along: Haseen, S.; Kroll, P., JEurCerSoc **2023**, 43, 1432-1441.). In that work, we show that a far simpler potential is already able to "reproduce" many experimental trends. Leimeroth et al. **2024** (we cite this "Early Access paper") follow this approach as "validation" – we think that the more detailed spectroscopic data (vibrations; outcome of ^{29}Si-NMR) is at least of equal rigor.

3. Long-Term Stability Analysis: Given the promising results shown, a study on the long-term stability and reliability of these MLIPs over extended periods and under various environmental conditions could further solidify their utility in industrial applications.

"Industrial applications" will require simulation times that are not accessible for atomistic simulations.
However, we were approached to consider performing "long-term simulations" in the micro-second range for "nano-meter-sized models" related to semiconductor circuitry. Such a "real-world application" will (would) require several months of simulation using 512 cores for just a single completed trajectory. Moreover, an expert researcher is required to attend and supervise these simulations. This is rather costly …
We think that – currently – it is more efficient for us as researchers to spend time on further method development and MLIP improvement.

Many thanks again for the comments. Along with our response we send a revised version of the manuscript.

With kindest regards

PETER KROLL

For Peer Review